IOPscience iopscience.iop.org

Home Search Collections Journals About Contact us My IOPscience

Structural ordering of interacting dimers on a square lattice

This article has been downloaded from IOPscience. Please scroll down to see the full text article.

1993 J. Phys. A: Math. Gen. 26 6847

(http://iopscience.iop.org/0305-4470/26/23/029)

View the table of contents for this issue, or go to the journal homepage for more

Download details:
IP Address: 171.66.16.68
The article was downloaded on 01/06/2010 at 20:13

Please note that terms and conditions apply.

J. Phys. A: Math. Gen. 26 (1993) 6847–6877. Printed in the UK

# Structural ordering of interacting dimers on a square lattice

A J Phares†, F J Wunderlich†, J D Curley† and D W Grumbine Jr‡

† Department of Physics, Mendel Hall, Villanova University, Villanova, PA 19085-1699, USA
‡ Department of Physics, Building 16, Lehigh University, Bethlehem, PA 18015, USA

Received 23 June 1993, in final form 2 August 1993

**Abstract.** We study the entropy of dimers on a semi-infinite $M \times N$ square lattice ($N \to \infty$) with lattice interaction energy per dimer $\mu_1$ and nearest-neighbour interaction energy $\mu_2$. Numerical computations based on recursive transfer matrices show that for $M = 1$, 2, 3, 4 and 5, and under certain conditions, the constant-$\mu_2$ curves of the entropy as a function of the coverage $\theta_1$ and the fraction $\theta_2'$ of the maximum number of possible nearest neighbours, merge into a single curve forming arches that meet at cusps. At the highest points of these arches, the interaction energies are in the ratio of small whole numbers. Based on the analysis of the configurations at the cusps, we extrapolate the results to the infinite two-dimensional lattice ($M = \infty$) and obtain the location of at least two cusps. The first cusp occurs at $\theta_1 = 1/2$, $\theta_2' = 0$ and zero entropy, and the second at $\theta_1 = 2/3$, $\theta_2' = 2/9$ and an entropy of 0.102.

## 1. Introduction

Dimer statistics has been a fascinating and intriguing problem for decades [1]. Applications include the study of a lattice gas, the Ising problem and the adsorption of diatomic molecules on surfaces. A comprehensive review of this work may be found in the excellent book by Baxter [2]. The thermodynamics of dimers on periodic lattices may be obtained from the knowledge of the occupational degeneracy of dimers partially covering the lattice [3, 4]. Studies at full coverage were made for periodic [5] and aperiodic [6] lattices using exact and approximate methods; others included dimers on 2- and 3-dimensional arrays, with and without orientation-dependent energies [7]. Recursive relations for the composite occupational degeneracy were obtained for dimer–dimer and vacancy–vacancy nearest neighbours, on lattices of one and two strips of $N$ sites [8].

An $M \times N$ square lattice has $N$ horizontal rows each containing $M$ sites. Dimers occupy two nearest-neighbour sites and can be vertical or horizontal; but a site cannot be occupied by more than one end of a dimer. The only interaction energies are those between a dimer and the lattice ($\mu_1$), and between two nearest neighbour ends of two dimers ($\mu_2$). We present a method of obtaining the partition function of this system of dimers in terms of the eigenvalues of a transfer matrix, $\mathbf{T}(M)$, whose rank depends on the width $M$ of the lattice. In the thermodynamic limit ($N \to \infty$), the partition function is shown to depend only on the largest eigenvalue of $\mathbf{T}(M)$. The knowledge of $\mathbf{T}(M)$ provides all the thermodynamic properties of the system.

Let $x_1$ and $x_2$ be the absolute activities associated with the interaction energies $\mu_1$ and $\mu_2$, namely,

$$x_1 = \exp(\mu_1/k_B T) \qquad x_2 = \exp(\mu_2/k_B T) \tag{1.1}$$

0305-4470/93/236847+31$07.50 © 1993 IOP Publishing Ltd 

where $k_B$ is Boltzmann's constant and T the absolute temperature at equilibrium. The width $M$ of the lattice is kept fixed, its length $N$ is allowed to vary and, in the thermodynamic limit, it becomes infinite. The degeneracy $A_1(q, b, M, N)$ is the number of ways $q$ dimers with $b$ nearest neighbours can be distributed on the $M \times N$ lattice and depends on $M$. However, the $M$-dependence will not be made explicit in either the degeneracy or any of the derived quantities. The grand canonical partition function of the system is

$$\Delta_N(x_1, x_2) = \sum_{q,b} A_1(q, b, N) x_1^q x_2^b \tag{1.2}$$

and the partition function follows as

$$Z_N(x_1, x_2) = [\Delta_N(x_1, x_2)]^{1/MN} \tag{1.3}$$

with its thermodynamic limit given by

$$Z_N(x_1, x_2) = \lim_{N\to\infty} Z_N(x_1, x_2) = \lim_{N\to\infty} [\Delta_N(x_1, x_2)]^{1/MN}. \tag{1.4}$$

The average number $\langle q \rangle$ of dimers at equilibrium is

$$\langle q \rangle = \frac{1}{\Delta_N} \sum_{q,b} q A_1(q, b, N) x_1^q x_2^b = MN \frac{x_1}{Z_N} \frac{\partial Z_N}{\partial x_1} \tag{1.5}$$

and the fraction $\theta_1$ of lattice sites occupied by dimers is

$$\theta_1 = \frac{2\langle q \rangle}{MN} = \frac{2x_1}{Z_N} \frac{\partial Z_N}{\partial x_1} \underset{N\to\infty}{\longrightarrow} \frac{2x_1}{Z} \frac{\partial Z}{\partial x_1}. \tag{1.6}$$

Similarly, with $\langle b \rangle$ representing the average number of nearest neighbours, one defines $\theta_2$ as

$$\theta_2 = \frac{2\langle b \rangle}{MN} = \frac{2x_2}{Z_N} \frac{\partial Z_N}{\partial x_2} \underset{N\to\infty}{\longrightarrow} \frac{2x_2}{Z} \frac{\partial Z}{\partial x_2}. \tag{1.7}$$

This quantity is in the range $[0, (3M-2)/M]$, thus, $\theta_2' = [M/(3M-2)]\theta_2$ is normalized and lies in the range [0,1]; it represents the fraction of the maximum number of nearest neighbours obtained at full coverage. The entropy per site divided by Boltzmann's constant (hereafter referred to as entropy) is then given by:

$$S_N = \ln Z_N - \tfrac{1}{2}\theta_1 \ln x_1 - \tfrac{1}{2}\theta_2 \ln x_2 \tag{1.8}$$

and its thermodynamic limit is denoted $S$. For given values of $x_2$, the entropy reaches an extremum when its derivative with respect to $x_1$ is zero. This occurs when the interaction energies are related according to:

$$\mu_1 + (\partial\theta_2/\partial\theta_1)_{x_2}\mu_2 = 0. \tag{1.9}$$

Section 2 summarizes the general method [4] of obtaining the partition function for any width $M$. Section 3 describes the construction of the transfer matrix $\mathsf{T}(1)$ and discusses the one-dimensional results ($M = 1$). In particular, constant $\mu_2$ curves of the entropy as a function of the coverage exhibit a cusp at the 2/3 coverage. Section 4 shows the extention of the one-dimensional technique to obtain the transfer matrix $\mathsf{T}(2)$. In Section 5 we obtain a recursive construction of $\mathsf{T}(M)$ for any $M > 2$. Section 6 describes a numerical technique in calculating the relevant thermodynamic quantities and analyses numerical results for $M = 2$, 3, 4 and 5. Several new cusps are discovered and $\theta_2'$ is found to be linearly related to $\theta_1$ in the regions between them. The subsequent relations derived between the interaction energies at the maxima of the entropy between the cusps are numerically verified. Section 7 is a study of the configurations at these cusps; it presents an extrapolation of the results to the infinite two-dimensional lattice. Section 8 gives the summary.

## 2. Partition function

'Restricted' or 'truncated' [4] $M \times N$ lattices are obtained by restricting the occupation of one or more sites in the first row. Subscript $t$ is used to enumerate lattices: the lattice for which no restriction is placed on the occupation of the first row is $t = 1$. With the degeneracy $A_t(q, b, N)$ we associate the generating function $G_t(x_1, x_2, y)$:

$$G_t(x_1, x_2, y) = \sum_{q,b,N} A_t(q, b, N) x_1^q x_2^b y^N. \tag{2.1}$$

By developing linearly coupled recursive relations among the $A_t$s, closed-form expressions for the generating functions are obtained as a ratio of two finite polynomials, $H_t(x_1, x_2, y)$ and $D(x_1, x_2, y)$ [3,4]. The polynomial $D(x_1, x_2, y)$ appearing in the denominator is the same for all $G_t$s. The generating function related to the grand canonical partition function, $\Delta_N(x_1, x_2)$, is the one associated with the unrestricted lattice; it is given by

$$G_1(x_1, x_2, y) = \sum_{q,b,N} \Delta_N(q, b, N) y^N = \frac{H_1(x_1, x_2, y)}{D(x_1, x_2, y)}. \tag{2.2}$$

In $D(x_1, x_2, y)$ we set $y = 1/z$, and call $R_j(x_1, x_2)$ the $j$th z-root of $D(x_1, x_2, 1/z)$, with $R_1(x_1, x_2)$ representing the largest root. This allows the factorization

$$D(x_1, x_2, y) = \alpha(x_1, x_2) \prod_j [1 - y R_j(x_1, x_2)] \tag{2.3}$$

so that

$$\frac{H_1(x_1, x_2, y)}{D(x_1, x_2, y)} = \frac{H_1(x_1, x_2, y)}{\alpha \prod_j [1 - y R_j(x_1, x_2)]} = \sum_j \frac{k_j(x_1, x_2)}{1 - y R_j(x_1, x_2)} \tag{2.4}$$

and $k_j(x_1, x_2)$ is:

$$k_j(x_1, x_2) = \lim_{y R_j \to 1} [1 - y R_j(x_1, x_2)] \frac{H_1(x_1, x_2, y)}{D(x_1, x_2, y)}. \tag{2.5}$$

The power-series expansion of $[1 - y R_j(x_1, x_2)]^{-1}$ yields

$$G_1(x_1, x_2, y) = \sum_N y^N \left[ \sum_j k_j(x_1, x_2) \Big( R_j(x_1, x_2) \Big)^N \right]. \tag{2.6}$$

In this summation, as follows from equation (2.2), the grand canonical partition function is the coefficient with $y^N$. Thus,

$$Z_N(x_1, x_2, y) = \left[ \sum_j k_j(x_1, x_2) \Big( R_j(x_1, x_2) \Big)^N \right]^{1/MN} \tag{2.7}$$

and the partition function in the thermodynamic limit follows:

$$Z_N(x_1, x_2, y = \lim_{N \to \infty} [R_1(x_1, x_2)]^{1/M} \Big[ \sum_j k_j (R_j / R_1)^N \Big]^{1/MN} = [R_1(x_1, x_2)]^{1/MN}. \tag{2.8}$$

## 3. The one-dimensional problem

In the one-dimensional problem ($M = 1$), there are three restricted lattices. Figure 1 provides a diagrammatic construction of recursive relations among the corresponding degeneracies. The lattice is represented by $N$ square cells, the center of each representing a lattice site. An unmarked cell corresponds to an unspecified state of occupation; a cell marked by a non-shaded circle is restricted to be vacant; and a cell marked by a shaded circle and a 'tail' specifies one end of a dimer occupying that cell, with the tail pointing in the direction of its other end. For the unrestricted lattice, there is only one arrangement with no dimers and no nearest neighbours, irrespective of the number of sites (including $N = 0$), so that

$$A_1(0, 0, N) = 1 \quad \text{for} \quad N \geqslant 0. \tag{3.1}$$

In figure 1($a$), $A_1(q, b, N)$ is represented by a lattice with all its cells left unmarked. The first cell can be either vacant or occupied by one end of a dimer. Thus, $A_1(q, b, N)$ is the sum of the number of arrangements with the first cell vacant, and the number of arrangements with the first two cells occupied by a dimer. In the first case, a vacancy cannot lead to a dimer–dimer nearest neighbour; and on the remaining $N - 1$ cells, the number of arrangements of $q$ dimers with $b$ nearest neighbours is the same as $A_1(q, b, N - 1)$. In the second case, a cell occupied by a dimer may lead to a nearest-neighbour configuration, and we label $t = 3$ the lattice having $N - 1$ cells, with its first cell occupied by the top of a dimer. Thus the number of arrangements in this second case is the same as that of $q - 1$ dimers with $b$ nearest neighbours on a restriced lattice of type $t = 3$ and having $N - 1$ cells, or $A_3(q - 1, b, N - 1)$. The first recursive relation valid for $N \geqslant 1$ is established (figure 1($a$)) as

$$A_1(q, b, N) = A_1(q, b, N - 1) + A_3(q - 1, b, N - 1) \tag{3.2}$$

with the initial conditions

$$A_3(0, 0, 0) = 0 \qquad A_3(-1, 0, 0) = 0 \qquad A_3(0, 0, N) = 1 \quad \text{for } N \geqslant 1. \tag{3.3}$$

The number of arrangements $A_3(q, b, N)$ shown in figure 1($b$) is the same as the number of arrangements of $q$ dimers on a lattice having $N - 1$ cells so that underneath the first cell there lies the top of a dimer. This restricted lattice is labelled $t = 2$, and a second recursive relation

$$A_3(q, b, N) = A_2(q, b, N - 1) \tag{3.4}$$

is obtained, valid for $N \geqslant 1$, with the initial conditions

$$A_2(0, 0, N) = 1 \qquad \text{for} \qquad N \geqslant 0. \tag{3.5}$$

Figure 1($c$) presents the recursive relation for $A_2(q, b, N)$. This number is the sum of the degeneracy with the first cell vacant, or $A_1(q, b, N - 1)$, and the degeneracy with the first two cells occupied by a dimer with its lower end neighbouring the top of a dimer. This last degeneracy is equivalent to $A_3(q - 1, b - 1, N - 1)$, and a third recursive relation valid for $N \geqslant 1$ is established:

$$A_2(q, b, N) = A_1(q, b, N - 1) + A_3(q - 1, b - 1, N - 1). \tag{3.6}$$

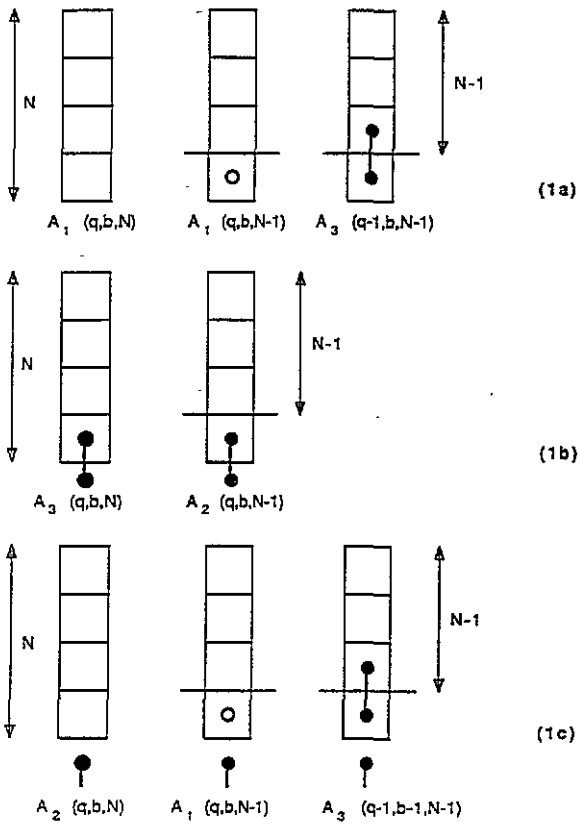


**Figure 1.** Diagrammatic representation of the recursive relations among the occupational degeneracies of dimers on the restricted lattices for the one-dimensional problem.

We associate with the above three restricted lattices three generating functions as specified by equation (2.1). We multiply both sides of each of equations (3.2), (3.4) and (3.6) by the quantity $x_1^q x_2^b y^N$. For given values of $N$ ($N > 1$) and $q$ ($q \leqslant$ integer part of $N/2$), we sum over all possible values of $b$. Then we sum over all possible values of $q$, keeping $N$ fixed, and finally sum over $N$. These operations yield [4]

$$G_1 - 1 = yG_1 + x_1yG_3 \qquad G_2 - 1 = yG_1 + x_1x_2yG_3 \qquad G_3 = yG_2 \tag{3.7}$$

which leads to the matrix formulation

$$\begin{bmatrix} 1-y & 0 & -x_1y \\ -y & 1 & -x_1x_2y \\ 0 & -y & 1 \end{bmatrix} \begin{bmatrix} G_1 \\ G_2 \\ G_3 \end{bmatrix} = \begin{bmatrix} 1 \\ 1 \\ 0 \end{bmatrix} \equiv QG \tag{3.8}$$

where $Q$ is the $3 \times 3$ matrix and $G$ is the column matrix whose elements are the generating functions. It then follows that $G_1$ is the ratio of two polynomials, $H_1(x_1, x_2, y)$, which is the sum of the cofactors of matrix elements $Q_{11}$ and $Q_{12}$, and $D(x_1, x_2, y)$, which is the determinant of $Q$, namely,

$$D(x_1, x_2, y) = x_1(x_2 - 1)y^3 - x_1x_2y^2 - y + 1. \tag{3.9}$$

The partition function is therefore obtained in terms of the $z$-roots of $D(x_1, x_2, 1/z)$ and, as expected, one recovers the cubic equation giving the solution of the one-dimensional system. A different formulation is achieved by observing that $Q$ is the sum of the identity matrix and a matrix whose elements have $y$ as a common factor, namely,

$$\left\{\begin{bmatrix}1 & 0 & 0\\ 0 & 1 & 0\\ 0 & 0 & 1\end{bmatrix} - y\begin{bmatrix}1 & 0 & x_1\\ 1 & 0 & x_1x_2\\ 0 & 1 & 0\end{bmatrix}\right\}\begin{bmatrix}G_1\\ G_2\\ G_3\end{bmatrix} = \begin{bmatrix}1\\ 1\\ 0\end{bmatrix}. \tag{3.10}$$

We define $\mathbf{T}(1)$ as

$$T(1) = \begin{bmatrix}1 & 0 & x_1\\ 1 & 0 & x_1x_2\\ 0 & 1 & 0\end{bmatrix} \tag{3.11}$$

and, with $z = 1/y$ and $I$ representing the identity matrix, we obtain

$$\{T(1) - zI\} = \begin{bmatrix}G_1\\ G_2\\ G_3\end{bmatrix} = \begin{bmatrix}-z\\ -z\\ 0\end{bmatrix}. \tag{3.12}$$

The $z$-roots of $D(x_1, x_2, 1/z)$ providing the partition function of the system are the singularities of the generating functions. According to equation (3.12), these singularities are the solutions of

$$\det\{T(1) - zI\} = 0. \tag{3.13}$$

The problem is reduced to obtaining the eigenvalues of $\mathbf{T}(1)$. The derivation of the transfer matrix $\mathbf{T}(1)$ continues to hold in the construction of the transfer matrices $\mathbf{T}(M)$ for $M > 1$.

The characteristic equation for $\mathbf{T}(1)$ is the cubic equation

$$-x_1(x_2 - 1) + x_1x_2z + z^2 - z^3 = 0 \tag{3.14}$$

readily solved in closed form, and reproducing the same $z$-roots as those of $D(x_1, x_2, 1/z)$, which we identify as $R_1$, $R_2$ and $R_3$. In the thermodynamic limit, from equation (2.8), the partition function of the one-dimensional system ($M = 1$) is the largest root $R_1$. The solution $R_1(x_1, x_2)$ is a well behaved function which increases smoothly with increasing values of its arguments. We compute the partial derivatives of $R_1$ with respect to the activities and find the properties

$$\frac{\partial R_1}{\partial x_1} = \frac{x_2(R_1 - 1) + 1}{3R_1^2 - 2R_1 - x_1x_2} \qquad \frac{\partial R_1}{\partial x_2} = \frac{x_1(R_1 - 1)}{3R_1^2 - 2R_1 - x_1x_2} \tag{3.15}$$

from which we obtain

$$\theta_1 = \frac{2R_1(R_1 - 1)}{3R_1^2 - 2R_1 - x_1x_2} \qquad \theta_2 = \frac{x_1x_2}{R_1^2}\theta_1. \tag{3.16}$$

The expression for the entropy follows from equation (1.8).

*Plot of $\theta_2'$ versus $\theta_1$*

We introduce dimensionless interaction energy parameters:

$$\bar{\mu}_1 = \log_{10} x_1 = \frac{\mu_1}{k_B T} \log_{10} e \qquad \bar{\mu}_2 = \log_{10} x_2 = \frac{\mu_2}{k_B T} \log_{10} e. \tag{3.17}$$

Figure 2 shows $\theta_2'$ versus $\theta_1$, with the constant $x_2$ curves labelled by the values of $\bar{\mu}_2$. For $\bar{\mu}_2 \gg 0$, the data falls almost along the line $\theta_2' = \theta_1$. This is justified analytically, since in that range $R_1 \equiv (x_1 x_2)^{1/2}$, and $\theta_2'$ is related to $\theta_1$ via equation (3.16). At $x_2 = 0$ ($\bar{\mu}_2 = -\infty$), there is an infinite nearest-neighbour repulsion and $\theta_2' = 0$, while $\theta_1$ increases from 0 to 2/3, as follows from equation (3.16). Indeed, the maximum possible coverage occurs by leaving one vacant site between two consecutive dimers. For $\bar{\mu}_2 \ll 0$, we observe the data points to fall along two segments: the section of the $\theta_1$-axis between 0 and 2/3, and the section of the line $\theta_2' = 3\theta_1 - 2$ where $\theta_1$ is in the range (2/3,1). The set of data points falling along the second segment corresponds to activities in the range $x_1 x_2 \gg 1$. Finally, all data points fall within the boundary of a triangle whose sides are $\theta_2' = 0$, $\theta_2' = \theta_1$ and $\theta_2' = 3\theta_1 - 2$. Structural ordering occurs at 2/3 coverage and can be analysed by studying the entropy of the system.

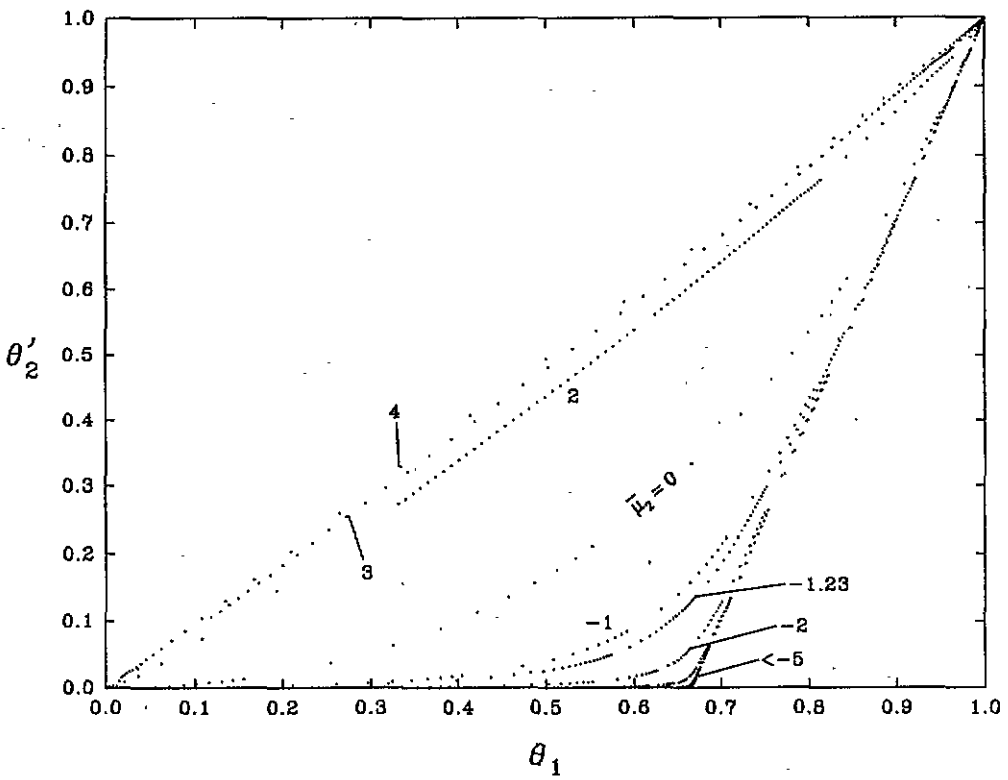


**Figure 2.** Plot of the fraction of maximum number of nearest neighbours versus the coverage for the one-dimensional lattice.

*Three-dimensional plot of S versus $\theta_1$ and $\theta_2'$*

This plot is shown in figure 3. The data is distributed on a dome-like surface which has two arches, one in the plane $\theta_2' = 0$ and the other in the plane $\theta_2' = 3\theta_1 - 2$. They meet to form a cusp at $S = 0$, $\theta_2' = 0$, $\theta_1 = 2/3$. The first arch is the entropy curve $x_2 = 0$ ($\bar{\mu}_2 = -\infty$). Its highest point is at $x_1 = 1$ ($\bar{\mu}_1 = 0$), where the entropy reaches the value $S_{max} = \ln(R_1)$, with $R_1$ being the largest root of $z^3 - z^2 - 1 = 0$. For $\bar{\mu}_2 < -5$, the entropy curves merge into a single curve consisting of the two arches. The highest point on the second arch will be considered later. Finally, the highest point of the dome is found on the curve $\bar{\mu}_2 = 0$ with the entropy reaching the value $S_{max} = \ln(R_1)$, where $R_1$ is the golden ratio [4]. These results are:

**Table 1.**

| $x_2$ | $S_{max}$ | $\theta_1$ | $\theta_2'$ |
|---|---|---|---|
| 0 | 0.382 245 078 | 0.388 508 011 | 0 |
| 1 | 0.481 218 250 | 0.552 786 405 | 0.211 145 618 |

Furthermore, at $x_2 = 1$ ($\bar{\mu}_2 = 0$) we find

$$\theta_2 = \frac{\theta_1^2}{2 - \theta_1} \qquad x_1 = \frac{\theta_1(2 - \theta_1)}{4(1 - \theta_1)^2}. \tag{3.18}$$

and the familiar expression for $S$ in terms of $\theta_1$ follows [4]. The first of the two equations in (3.18) is a new result which could not have been derived from our previous calculations [4].

For $\bar{\mu}_2 > 0$, the curves have one maximum asymptotically approaching zero as $\bar{\mu}_2$ becomes infinitely large. In that limit, we reach the base of the dome where $S = 0$ and $\theta_2' = \theta_1$.

Figure 3 also exhibits intermediate curves for $\bar{\mu}_2 = -1$, $-2$ etc, showing a local minimum gradually developing into a cusp. This minimum appears at $\bar{\mu}_2 < -1.23$. The curve corresponding to $\bar{\mu}_2 = -1.23$ is shown on the relevant graphs. All constant $\bar{\mu}_2$ curves, with $\bar{\mu}_2 < -5$, merge into two arches.

*Entropy as a function of the dimensionless interaction energies*

Figure 4 shows the plot of $S$ versus $\bar{\mu}_1$ and $\bar{\mu}_2$, and the planar constant $\bar{\mu}_2$ curves are identified. The curve at $\bar{\mu}_2 = -1.23$ has a maximum at $S = 0.405$ and $\bar{\mu}_1 = 0.176$, followed by a plateau, beyond which the entropy falls off to zero. In the plateau region, the entropy remains within 1% of 0.323 for maximum changes in lattice interaction energies of 35%, and changes in coverage varying from 68.6% to 77.8%. For $\bar{\mu}_2 < -1.23$, a local minimum begins to appear; the region between the two peaks on either side of this minimum broadens, and becomes almost flat, with $S \simeq 0$. When this occurs we are in the region of the cusp of figure 3, and the peaks correspond to the highest points of the two arches. For $\bar{\mu}_2 < -5$, we observe numerically that the second peak occurs at $x_2 x_1^{1/3} \simeq 1$, or at interaction energies related by

$$\mu_1 + 3\mu_2 = 0. \tag{3.19}$$

This can be derived analytically. Under the conditions stated above, the solution of equation (3.14) is given by

$$R_1 = \alpha x_1^{1/3} \qquad \alpha = \frac{1}{2^{1/3}}\left[\left(1 + \sqrt{\frac{23}{27}}\right)^{1/3} + \left(1 - \sqrt{\frac{23}{27}}\right)^{1/3}\right] \tag{3.20}$$

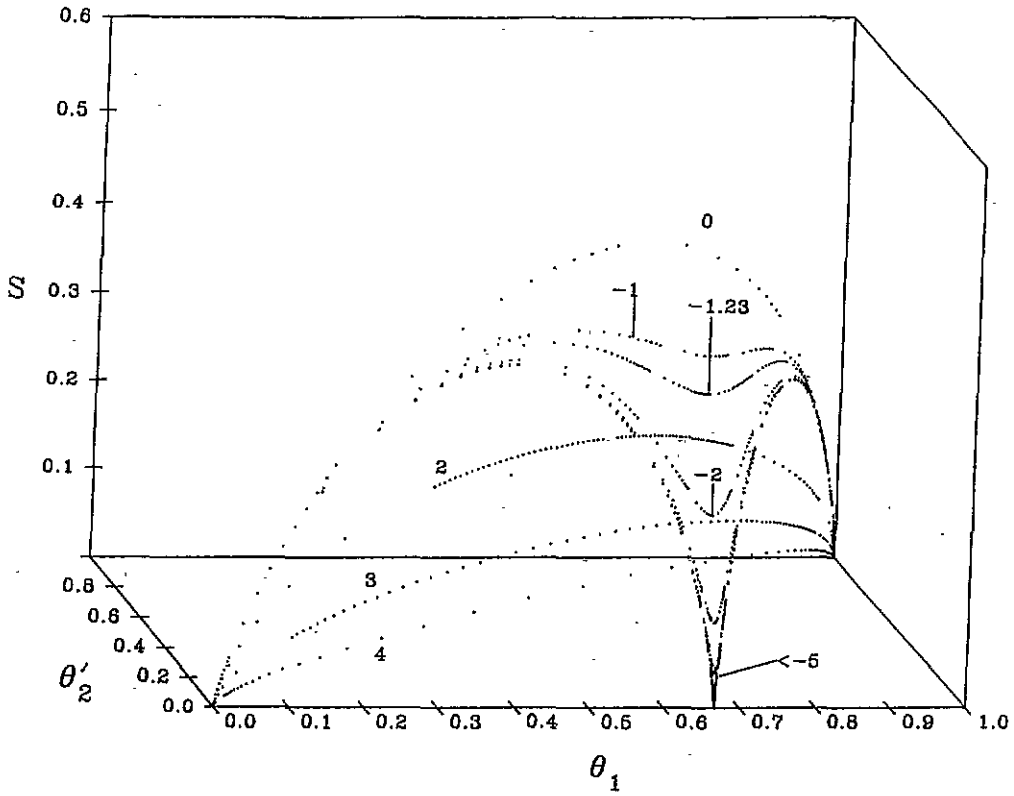


**Figure 3.** Plot of the entropy versus the coverage and the fraction of the maximum number of nearest neighbours for the one-dimensional lattice.

and the values of $\theta_1$, $\theta_2$ and $S$ follow:

$$\theta_1 = \frac{2(\alpha+1)}{\alpha(3\alpha^2-1)} \qquad \theta_2 = \frac{\theta_1}{\alpha^2} = 0.468\,973\,531 \tag{3.21}$$

$$S = \ln\alpha = 0.281\,199\,575. \tag{3.22}$$

This value of $S$ corresponds to the highest point of the second arch in figure 3, where condition (1.9) must hold. In this region, $\theta_2' = 3\theta_1 - 2$ and $(\partial\theta_2/\partial\theta_1)_{x_2} = 3$ showing that equation (3.19) follows from equation (1.9).

## 4. The transfer matrix T(2)

A first step in deriving a recursive relation for $\mathbf{T}(M)$ in terms of $\mathbf{T}(1)$ and $\mathbf{T}(2)$ is to propose a diagrammatic construction of matrix $\mathbf{T}(1)$, shown in figure 5, and generalize it to $\mathbf{T}(M)$. The row and column entries of $\mathbf{T}(1)$ are labelled by the first cell of the three possible restricted lattices. These are the ones for which there is: (1) a vacancy below the first cell (circle), (2) the top of a dimer below the first cell, and (3) the top of a dimer occupying the first cell. The diagrammatic construction of the $(ij)$ element of $\mathbf{T}(1)$ is based on placing the cell of the row entry (i) underneath the cell of the column entry $(j)$. When no matching is possible between the two states of occupancy, the corresponding matrix element is zero.

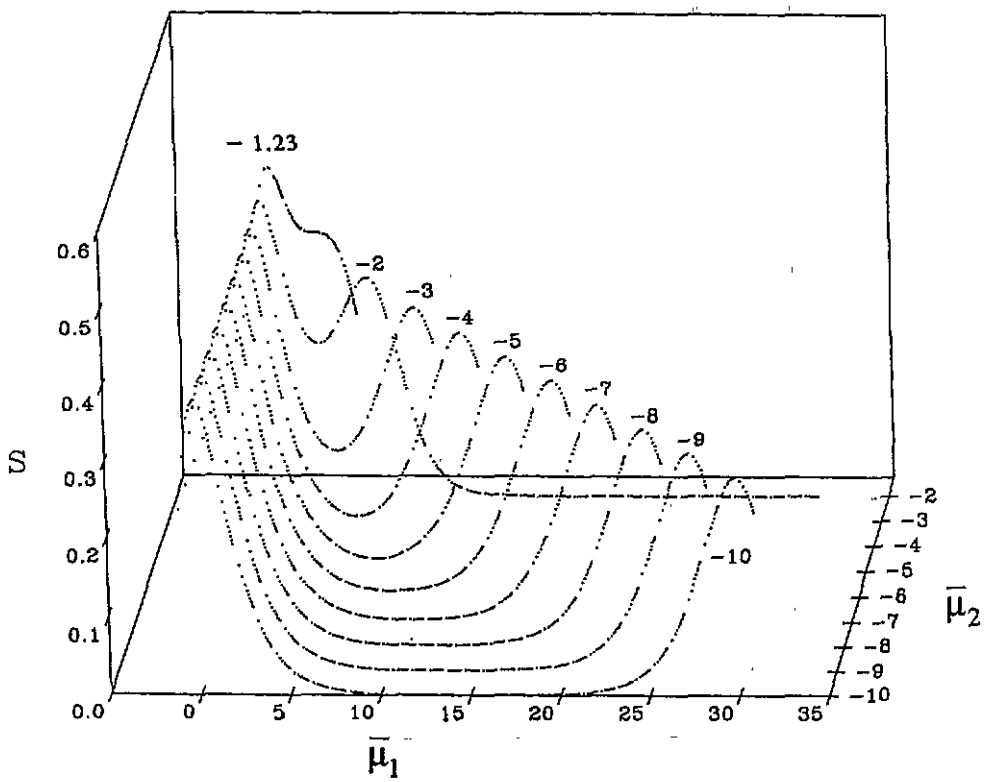


**Figure 4.** Plot of the entropy versus the dimensionless interaction energy parameters for the one-dimensional lattice.

This is the case for $T_{12}$, $T_{22}$, $T_{31}$ and $T_{33}$. The (1,1) element corresponds to placing a vacancy in the cell of the first row entry, which leads to a vacancy–vacancy nearest neighbour. There is zero energy associated with placing a vacancy on a lattice site and with nearest-neighbour vacancies, and therefore, the added activity is 1; this is the matrix element $T_{11}$. The (1,3) element corresponds to placing the bottom of a dimer in the cell of the first-row entry, leading to a lattice–dimer and vacancy–dimer nearest-neighbour interaction. The added activities are $x_1$ and 1, respectively, leading to a total activity $x_1 * 1$, and this is $T_{13}$. A matching of the cell of the second-row entry placed beneath the cell of the third-column entry is possible, leading to lattice–dimer and dimer–dimer nearest-neighbour interactions, with an added total activity $x_1 * x_2$, and this is $T_{23}$. Matching between the entries leading to $T_{32}$ is also possible with no added activities, and the corresponding element is 1. These rules will be shown to hold in constructing $\mathbf{T}(2)$ and higher-order transfer matrices.

To derive an expression for $\mathbf{T}(2)$, we need to identify restricted lattices (labelled $t$) and search for recursive relations among the arrangements $A_t(q, b, N)$ of $q$ dimers with $b$ nearest neighbours on the $2 \times N$ restricted lattices of type $t$.

The $A_1$ section of figure 6 refers to the number of arrangements $A_1(q, b, N)$ on the non-restricted lattice, where all possible occupations of the first row are considered. When the right cell is vacant, the left cell can be either vacant or occupied by the bottom of a dimer, generating two types of restricted lattices with $N - 1$ rows. The first corresponds to the two cells underneath the first row being vacant; this is equivalent to the original non-restricted

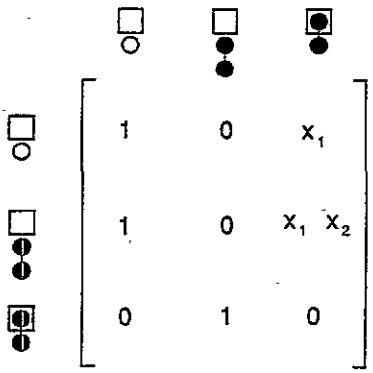


**Figure 5.** The transfer matrix for the one-dimensional problem.

lattice, since no dimer–dimer interactions can be established with vacancies. The second restricted lattice is labelled $t = 3$, as the ordering is an important factor in constructing the transfer matrix recursively. When the right cell of the first row is occupied by the bottom of a vertical dimer, the left cell is either a vacancy or is occupied by the bottom of another vertical dimer. These diagrams lead to two new restricted lattices, labelled $t = 7$ and $t = 9$, respectively. The last possible occupancy of the first row is the one for which the cells are occupied by a horizontal dimer, leading to the restricted lattice labelled $t = 10$. The first recursive relation is then established:

$$A_1(q, b, N) = A_1(q, b, N-1) + A_3(q-1, b, N-1) + A_7(q-1, b, N-1) + A_9(q-2, b-1, N-1) + A_{10}(q-1, b, N-1). \tag{4.1}$$

The $A_3$ section of figure 6 refers to the number of arrangements $A_3(q, b, N)$ and exhibits two new restricted lattices labelled $t = 2$ and $t = 8$, respectively, leading to the recurrence relation:

$$A_3(q, b, N) = A_2(q, b, N-1) + A_8(q-1, b, N-1). \tag{4.2}$$

The remaining relations are derived in a similar way, and ten restricted $2 \times N$ lattices are found with which we associate ten generating functions $G_t(x_1, x_2, y)$. Not shown in figure 6 are the diagrams leading to the relations for $A_8(q, b, N)$ and $A_{10}(q, b, N)$. The recurrence relations among the ten degeneracies provide a set of ten linear equations among the $G$s, leading to a matrix $Q$ as in equation (3.8) depending on $x_1$, $x_2$ and $y$. The matrix $Q$ provides a transfer matrix, $\mathsf{T}(2)$, of rank ten depending only on the activities. Figure 7 is matrix $\mathsf{T}(2)$ with its row and column entries labelled according to the configurations of the first row of the ten restricted lattices. The order hierarchy for choosing the state of occupancy *below* the first cell to the far right in the first row of the lattice is:

(a) a vacancy, or state $\alpha = 1$,

(b) the top of a vertical dimer, or state $\alpha = 2$,

(c) the bottom of a vertical dimer, or state $\alpha = 3$, or

(d) the right end of a horizontal dimer, or state $\alpha = 4$.

Next, we consider the occupancy below the second cell to the far right (also the last, since $M = 2$) in the first row of the lattice. For each of the states designated $\alpha = 1$, 2 and 3, this occupancy could be a vacancy, the top of a dimer, or the bottom of a dimer, in this order.

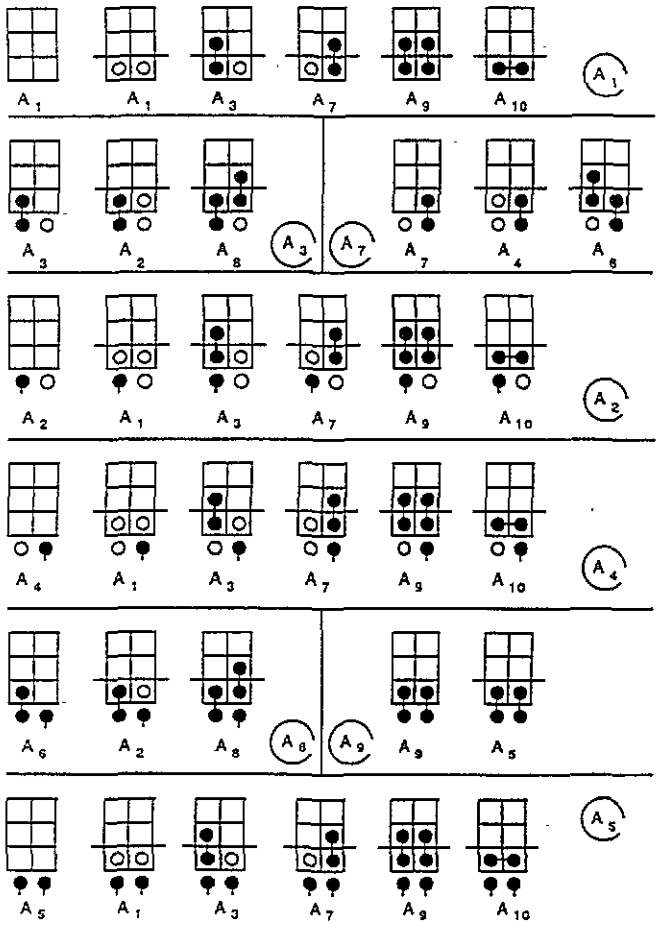


**Figure 6.** Diagrammatic representation of the recursive relations among the occupational degeneracies of dimers on the restricted lattices associated with the $2 \times N$ lattice.

For the state designated $\alpha = 4$, the two cells below the first row of sites are occupied by a horizontal dimer. Thus, we have accounted for all ten configurations. As shown in figure 7, $\mathbf{T}(2)$ is divided into 16 blocks, $\mathbf{B}_{\alpha\beta}$, where indices $\alpha$ and $\beta$ each refers to one of the four states of occupancy mentioned above. All elements of blocks $\mathbf{B}_{12}$, $\mathbf{B}_{22}$, $\mathbf{B}_{31}$, $\mathbf{B}_{33}$, $\mathbf{B}_{34}$ and $\mathbf{B}_{42}$ are zero. Blocks $\mathbf{B}_{11}$ and $\mathbf{B}_{21}$ are equal to $\mathbf{T}(1)$, and other relations are

$$\mathbf{B}_{13} = x_1\mathbf{B}_{32} \qquad \mathbf{B}_{23} = x_1x_2\mathbf{B}_{32} \qquad \mathbf{B}_{24} = x_2\mathbf{B}_{14}. \tag{4.3}$$

The elements of $\mathbf{T}(2)$ are products of activities, one or zero, which is always true for any $\mathbf{T}(M)$. In exactly the same manner as was done for $\mathbf{T}(1)$, the diagrammatic construction of matrix element $T_{ij}(2)$ follows from placing the cells of the row entry $(i)$ underneath the cells of the column entry $(j)$, where $i$ and $j$ run from 1 to 10. The element $T_{ij}(2)$ is zero when no matching is possible, otherwise it is a product of any added activities. When matching is possible with no added activity, then $T_{ij}(2) = 1$. Therefore, there is no further need to investigate degeneracies for lattice width greater than 2 in order to derive the corresponding transfer matrices.

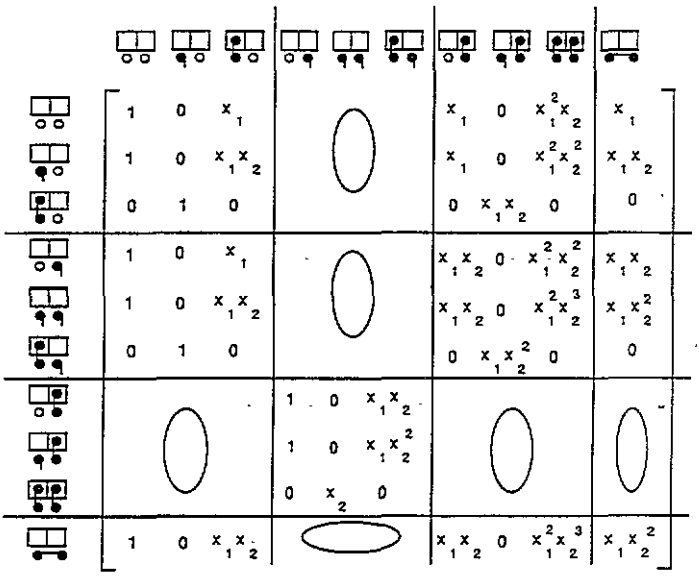

**Figure 7.** The transfer matrix for the $2 \times N$ lattice.

A larger number of configurations would have been necessary if we had originally assigned a non-zero energy for vacancy–dimer and vacancy–vacancy nearest neighbours.

## 5. The transfer matrix $\mathbf{T}(M)$

The generalization to $M > 2$ is based on dividing the transfer matrix $\mathbf{T}(M)$ into 16 blocks (see figure 8), according to the four states of occupancy just underneath the cell furthest to the right on the first row of the lattice, as done for $M = 2$. The matrix entries are labelled by the drawings of these configurations. The rank $D(M)$ of $\mathbf{T}(M)$ is the number of restricted lattices. For each of the three states of occupancy below the first cell to the far right, $\alpha = 1$, 2 or 3; the total number of restricted lattices is $D(M-1)$. When the state of occupancy is $\alpha = 4$, the number of restricted lattices is $D(M-2)$. This establishes the relation

$$D(M) = 3D(M-1) + D(M-2) \tag{5.1}$$

with the initial conditions $D(0) = 1$ and $D(1) = 3$.

Block matrices $\mathbf{B}_{\alpha\beta}$ with $\alpha$ and $\beta$ taking the values 1, 2 or 3 are all square matrices having the same rank, $D(M-1)$. The block matrix $\mathbf{B}_{44}$ is also a square matrix and its rank is $D(M-2)$. The blocks $\mathbf{B}_{\alpha 4}$ are $D(M-1) \times D(M-2)$ matrices, and blocks $\mathbf{B}_{4\beta}$ are $D(M-2) \times D(M-1)$ matrices. By placing the cells of the row entry ($\alpha$) underneath the cells of the column entry ($\beta$), the matching of the configurations allows one to obtain the general features of $\mathbf{T}(M)$ as indicated on figure 4, namely,

$$\mathbf{B}_{11} = \mathbf{B}_{21} = \mathbf{T}(M-1) \qquad \mathbf{B}_{32} = \mathbf{P}(M-1) \tag{5.2a}$$

$$\mathbf{B}_{13} = x_1\mathbf{P}(M-1) \qquad \mathbf{B}_{23} = x_1x_2\mathbf{P}(M-1) \qquad \mathbf{B}_{44} = x_1x_2^2\mathbf{P}(M-2) \tag{5.2b}$$

$$\mathbf{B}_{23} = \mathbf{K}(M-1) \qquad \mathbf{B}_{24} = x_1x_2\mathbf{K}(M-1) \tag{5.2c}$$

$$\mathbf{B}_{41} = \mathbf{L}(M-2) \qquad \mathbf{B}_{43} = x_1x_2\mathbf{J}(M-2). \tag{5.2d}$$

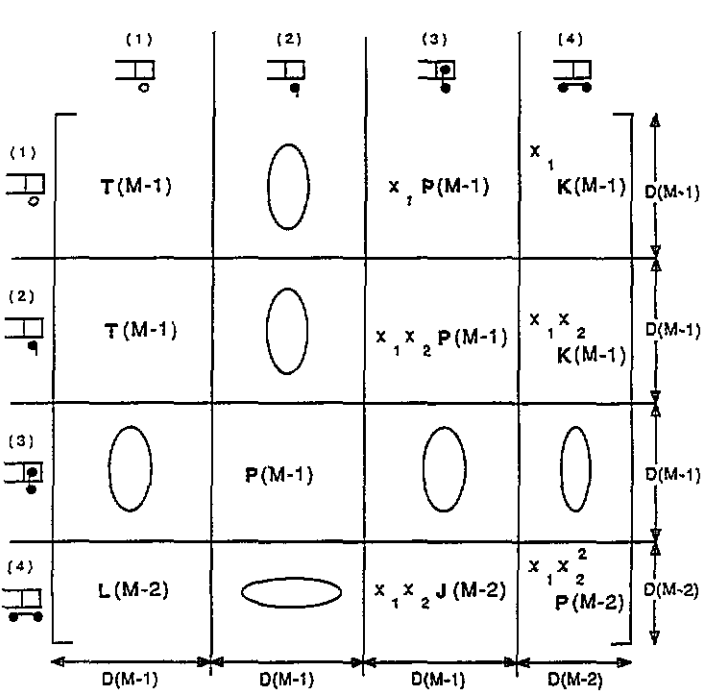


**Figure 8.** The general structure of the transfer matrix for the $M \times N$ lattice.

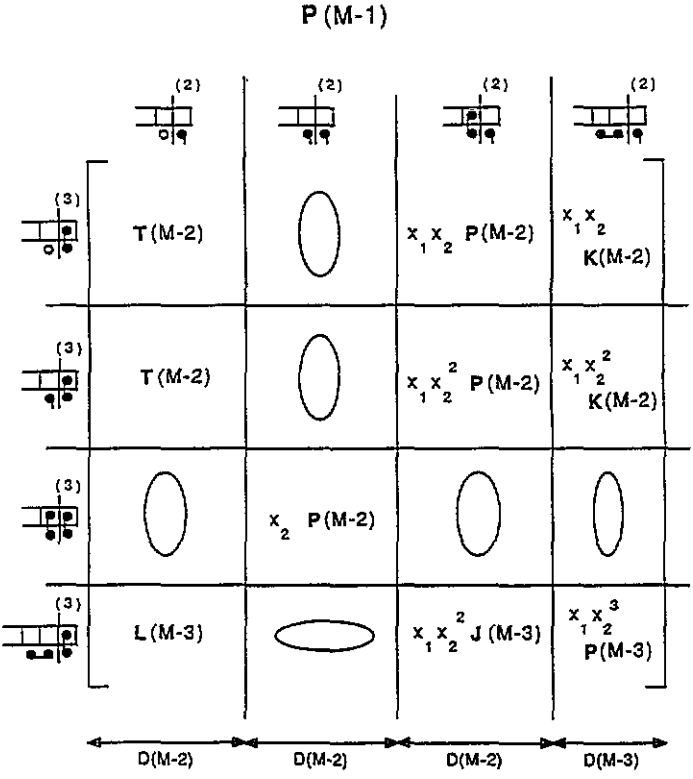


**Figure 9.** Recursive construction of the P matrix.

All other block matrices are zero because no matching is possible.

Assume that we know the transfer matrix $\mathbf{T}(M-1)$ associated with the $(M-1)\times N$ lattice. According to the general features indicated by equations (5.2), this requires the knowledge of matrices $\mathbf{T}(M-2)$, $\mathbf{P}(M-2)$, $\mathbf{K}(M-2)$, $\mathbf{L}(M-3)$ and $\mathbf{J}(M-3)$. This is not sufficient to construct the matrix $\mathbf{T}(M)$, since we do not know $\mathbf{P}(M-1)$, $\mathbf{K}(M-1)$, $\mathbf{L}(M-2)$ and $\mathbf{J}(M-2)$. However, by inspecting the $\mathbf{T}$ matrix for $M=2$, we find the initial values:

$$\mathbf{P}(0)=1 \qquad \mathbf{P}(1)=\begin{bmatrix}1 & 0 & x_1x_2\\ 1 & 0 & x_1x_2^2\\ 0 & x_2 & 0\end{bmatrix} \qquad \mathbf{K}(1)=\begin{bmatrix}1\\ x_2\\ 0\end{bmatrix} \tag{5.3}$$

$$\mathbf{J}(0)=\begin{bmatrix}1 & 0 & x_1x_2^2\end{bmatrix} \qquad \mathbf{L}(0)=\begin{bmatrix}1 & 0 & x_1x_2\end{bmatrix}.$$

Higher-order $\mathbf{P}$, $\mathbf{K}$, $\mathbf{J}$ and $\mathbf{L}$ matrices are obtained recursively, making use of the diagrammatic construction introduced above.

The matrix $\mathbf{P}(M-1)$ corresponds to the row entry with the first cell to the far right in state $\alpha=3$, and to the column entry with the first cell to the far right in state $\beta=2$. Figure 9 shows that the $\mathbf{P}$ matrix may again be divided into 16 block matrices. The four row and column entries of these new blocks correspond to the four possible states of occupation below the second cell from the far right. Ten of these block matrices are square, nine of them of rank $D(M-2)$ and the last of rank $D(M-3)$. The remaining block matrices are of the $\mathbf{K}$, $\mathbf{L}$ or $\mathbf{J}$ types. Again, the diagrammatic construction enables one to obtain the structure of the block matrices making up $\mathbf{P}(M-1)$. The results presented in figure 9 show that $\mathbf{P}(M-1)$ is constructed from the knowledge of matrices $\mathbf{T}(M-2)$, $\mathbf{P}(M-2)$,

K(M-1)

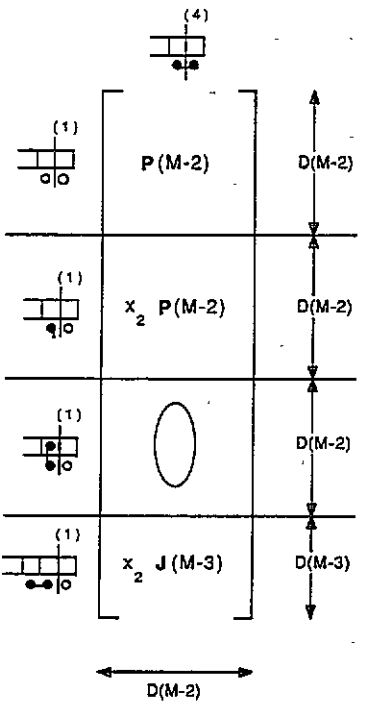


**Figure 10.** Recursive construction of the $\mathbf{K}$ matrix.

**P**($M-3$), **K**($M-2$), **L**($M-3$) and **J**($M-3$). In this manner, the block matrix **P**(2) which appears in the expression of **T**(3) is given in terms of **T**(1), **P**(1), **P**(0), **K**(1), **L**(0) and **J**(0); all these are listed in equation (5.3).

The constructions of **K**($M-1$), **L**($M-2$) and **J**($M-2$) are presented in figures 10, 11 and 12, respectively; this completes the recursive construction of the transfer matrix.

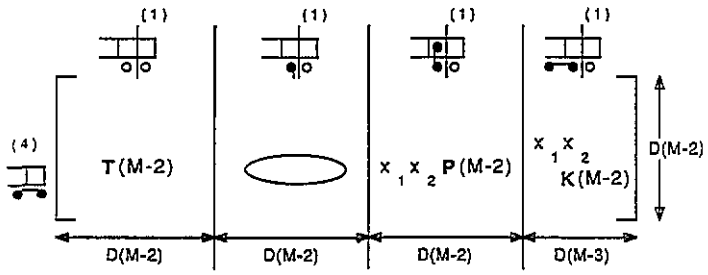


**Figure 11.** Recursive construction of the **L** matrix.

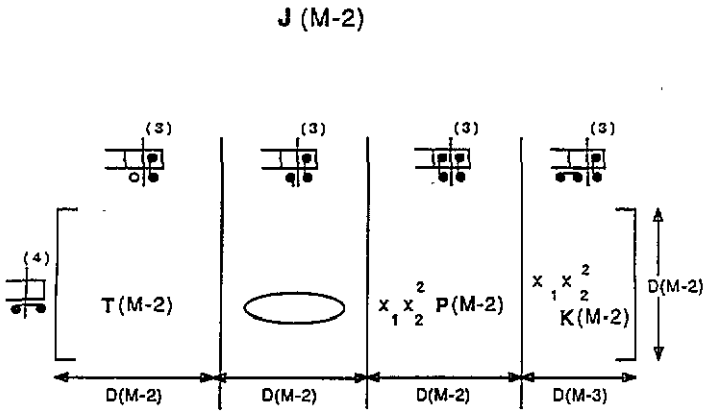


**Figure 12.** Recursive construction of the **J** matrix.

## 6. Numerical results for lattice widths M = 2, 3, 4 and 5

The rank of the transfer matrices are 10, 33, 109 and 360 for lattice widths $M = 2$, 3, 4 and 5, respectively. Computer-programming the recursive relations is the only practical way of obtaining these matrices. For a given $M$ and the numerical values of the activities $x_1$ and $x_2$, the largest eigenvalue of the transfer matrix, $R_1(x_1, x_2) \equiv R_{00}$, was determined using EISPACK on the Cray C90 at the Pittsburgh Supercomputing Center. As follows from equations (1.6)–(1.8) and (2.8), the entropy at these activities is

$$S(x_1, x_2) = \frac{1}{M} \ln R_{00} - \frac{1}{2}\theta_1 \ln x_1 - \frac{1}{2}\theta_2 \ln x_2 \tag{6.1}$$

$$\theta_1(x_1, x_2) = \frac{2x_1}{M R_{00}} \frac{\partial R_{00}}{\partial x_1} \qquad \theta_2(x_1, x_2) = \frac{2x_2}{M R_{00}} \frac{\partial R_{00}}{\partial x_2}. \tag{6.2}$$

The derivatives of the eigenvalue with respect to the activities at the evaluation point $(x_1, x_2)$ are computed numerically by evaluating the transfer matrix at eight neighbouring evaluation points $(x_1 \pm h_1, x_2)$, $(x_1, x_2 \pm h_2)$, $(x_1 \pm 2h_1, x_2)$ and $(x_1, x_2 \pm 2h_2)$. For sufficiently small values of $h_1$ and $h_2$, the corresponding largest eigenvalues, $R_{\pm 1,0}$, $R_{0,\pm 1}$, $R_{\pm 2,0}$ and $R_{0,\pm 2}$ are computed again using EISPACK and the derivatives are approximated by:

$$\frac{\partial R_{00}}{\partial x_1} \equiv \frac{1}{12h_1}\left[8(R_{1,0} - R_{-1,0}) - (R_{2,0} - R_{-2,0})\right] \tag{6.3a}$$

$$\frac{\partial R_{00}}{\partial x_2} \equiv \frac{1}{12h_2}\left[8(R_{0,1} - R_{0,-1}) - (R_{0,2} - R_{0,-2})\right]. \tag{6.3b}$$

The quantities $h_1$ and $h_2$ were adjusted to insure that our final results were accurate to six significant figures.

*Plot of $\theta_2'$ versus $\theta_1$*

The fraction $\theta_2'$ of the maximum number of nearest neighbours is a normalized quantity equal to $\theta_2$ only for $M = 1$, since

$$\theta_2' = \frac{M}{3M-2}\theta_2. \tag{6.4}$$

Figures 13, 14, and 15 are the plots of $\theta_2'$ versus $\theta_1$, for $M = 2$, 3, and 4, respectively. The data points for given values of $x_2$ are distributed along curves labelled by $\bar{\mu}_2$. For $\bar{\mu}_2 > 0$,

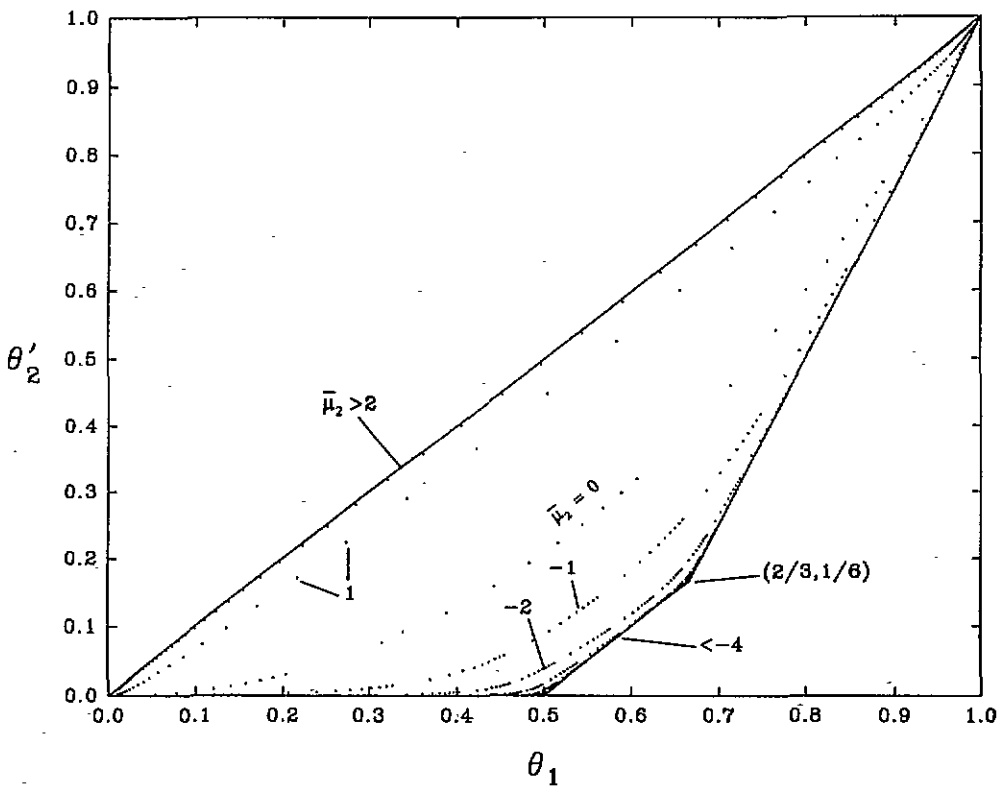


**Figure 13.** Plot of the fraction of the maximum number of nearest neighbours versus the coverage for the lattice of width $M = 2$.

the curves approach an *upper* boundary made of the line $\theta_2' = \theta_1$, as in the one-dimensional case. For $\bar{\mu}_2 < 0$, the curves approach a *lower* boundary made of three segments for $M = 2$, and four segments for $M = 3$ and 4. In all three cases, one of these sections is the portion (0, 1/2) of the $\theta_1$ axis, and the remaining segments are portions of the lines whose equations are numerically determined and listed in table 2. The plot $\theta_2'$ versus $\theta_1$ for $M = 5$ shows the existence of two energy ranges, $-7 < \bar{\mu}_2 < -3$ and $-\infty < \bar{\mu}_2 < -15$, where the points fall along the portion (0, 1/2) of the $\theta_1$-axis, and along either three or four other segments, as shown in table 2. Figure 16 shows the data collected for $\bar{\mu}_2 = -5$, $-10$, and $-20$ in the entire range of possible coverages. Figure 17 is an enlargement of figure 16 in the range $0.58 \leqslant \theta_1 \leqslant 0.62$ which shows a noticeable change in the lower boundary: the points for $\bar{\mu}_2 = -5$ lie on a straight line, while those for $\bar{\mu}_2 = -20$ lie on two straight lines intercepting at $\theta_1 = 3/5$. In all cases considered, the structural ordering expected to occur at the vertices of the lower boundary are analysed by studying the entropy of the system.

*Cusps in the entropy curves and energy changes about the cusps*

For $M = 1$, we presented the 3D plot of $S$ versus $\theta_1$ and $\theta_2'$. Figure 18 is an example of the projection of the entropy surface onto the $S$ versus $\theta_1$ plane in the case $M = 4$ which exhibits four arches and three cusps. The cusps correspond to the vertices of the lower boundary mentioned above. The corresponding data for $M = 5$ are presented in figure 19 with $\bar{\mu}_2 = -5$, $-10$ and $-20$. This figure shows a new cusp at the 3/5 coverage developing between two cusps *already* present at $\bar{\mu}_2 = -5$. This development was not observed in any previous case. We order the cusps by increasing values of the coverage and summarize

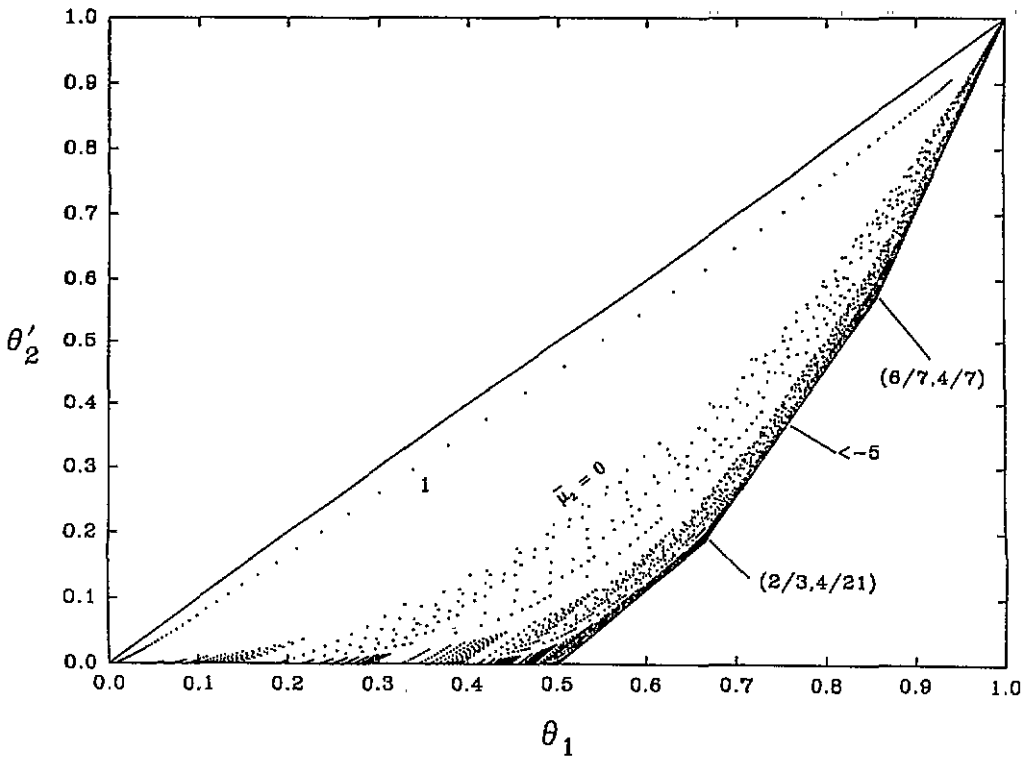


**Figure 14.** Plot of the fraction of the maximum number of nearest neighbours versus the coverage for the lattice of width $M = 3$.

**Table 2.** Equations of the segments making up the lower boundaries of the plots shown in figures 2, 13, 14, 15, 16, and 17.

| | | | | |
|---|---|---|---|---|
| $M = 1$ | $\theta_2' = 3\theta_1 - 2$ | | | |
| $-\infty < \bar{\mu}_2 < -7$ | $2/3 \leqslant \theta_1 \leqslant 1$ | | | |
| $M = 2$ | $2\theta_2' = 2\theta_1 - 2$ | $2\theta_2' = 5\theta_1 - 3$ | | |
| $-\infty < \bar{\mu}_2 < -7$ | $1/2 \leqslant \theta_1 \leqslant 2/3$ | $2/3 \leqslant \theta_1 \leqslant 1$ | | |
| $M = 3$ | $7\theta_2' = 8\theta_1 - 4$ | $7\theta_2' = 14\theta_1 - 8$ | $\theta_2' = 3\theta_1 - 2$ | |
| $-\infty < \bar{\mu}_2 < -7$ | $1/2 \leqslant \theta_1 \leqslant 2/3$ | $2/3 \leqslant \theta_1 \leqslant 6/7$ | $6/7 \leqslant \theta_1 \leqslant 1$ | |
| $M = 4$ | $5\theta_2' = 6\theta_1 - 3$ | $5\theta_2' = 9\theta_1 - 5$ | $5\theta_2' = 14\theta_1 - 9$ | |
| $-\infty < \bar{\mu}_2 < -7$ | $1/2 \leqslant \theta_1 \leqslant 2/3$ | $2/3 \leqslant \theta_1 \leqslant 4/5$ | $4/5 \leqslant \theta_1 \leqslant 1$ | |
| $M = 5$ | $13\theta_2' = 16\theta_1 - 8$ | $13\theta_2' = 25\theta_1 - 14$ | $13\theta_2' = 35\theta_1 - 22$ | |
| $-7 < \bar{\mu}_2 < -3$ | $1/2 \leqslant \theta_1 \leqslant 2/3$ | $2/3 \leqslant \theta_1 \leqslant 4/5$ | $4/5 \leqslant \theta_1 \leqslant 1$ | |
| $M = 5$ | $13\theta_2' = 15\theta_1 - 7.5$ | $13\theta_2' = 17.5\theta_1 - 9$ | $13\theta_2' = 25\theta_1 - 14$ | $13\theta_2' = 35\theta_1 - 22$ |
| $-\infty < \bar{\mu}_2 < -15$ | $1/2 \leqslant \theta_1 \leqslant 3/5$ | $3/5 \leqslant \theta_1 \leqslant 2/3$ | $2/3 \leqslant \theta_1 \leqslant 4/5$ | $4/5 \leqslant \theta_1 \leqslant 1$ |

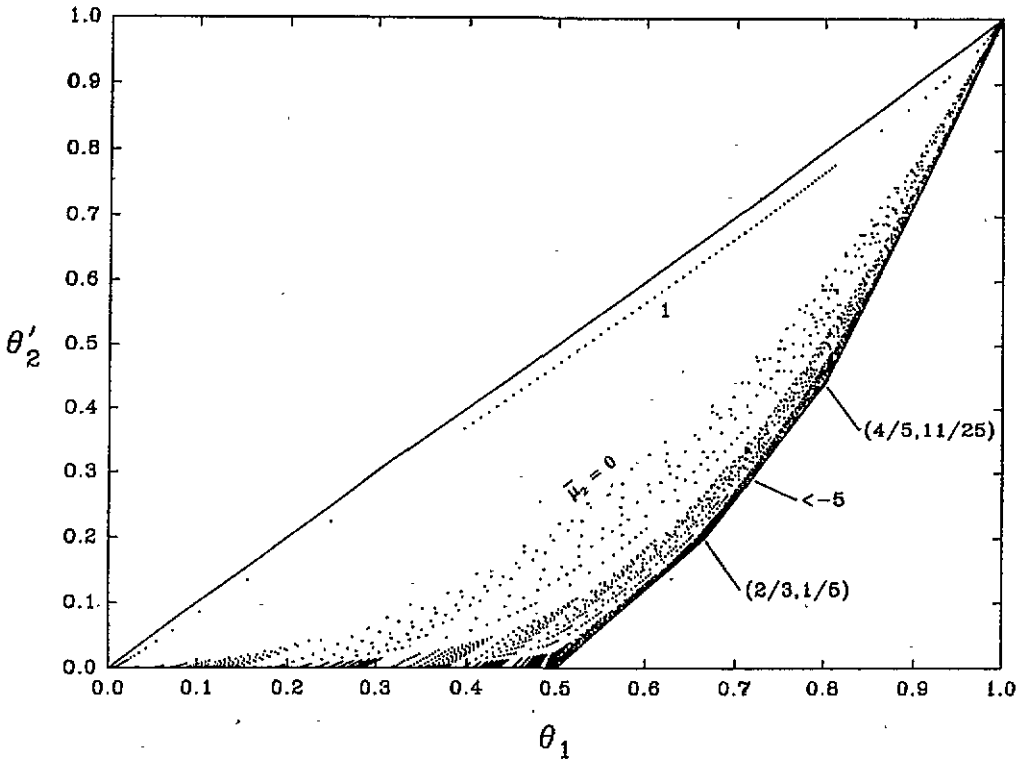


**Figure 15.** Plot of the fraction of the maximum number of nearest neighbours versus the coverage for the lattice of width $M = 4$.

their pertinent features in table 3. In all cases, the first arch is the $x_2 = 0$ curve ($\bar{\mu}_2 = -\infty$) with $\theta_2' = 0$. For $-\infty < \bar{\mu}_2 < -15$, the data show all the constant $\bar{\mu}_2$ curves merging into a single curve consisting of the 3, 4, or 5 arches, depending on the value of $M$. The pertinent features of the highest points of the arches are listed in tables 3 and 4.

At a cusp, the entropy is not always zero; however, it takes a tremendous amount of lattice interaction energy to change the order of the system. As an example of how the

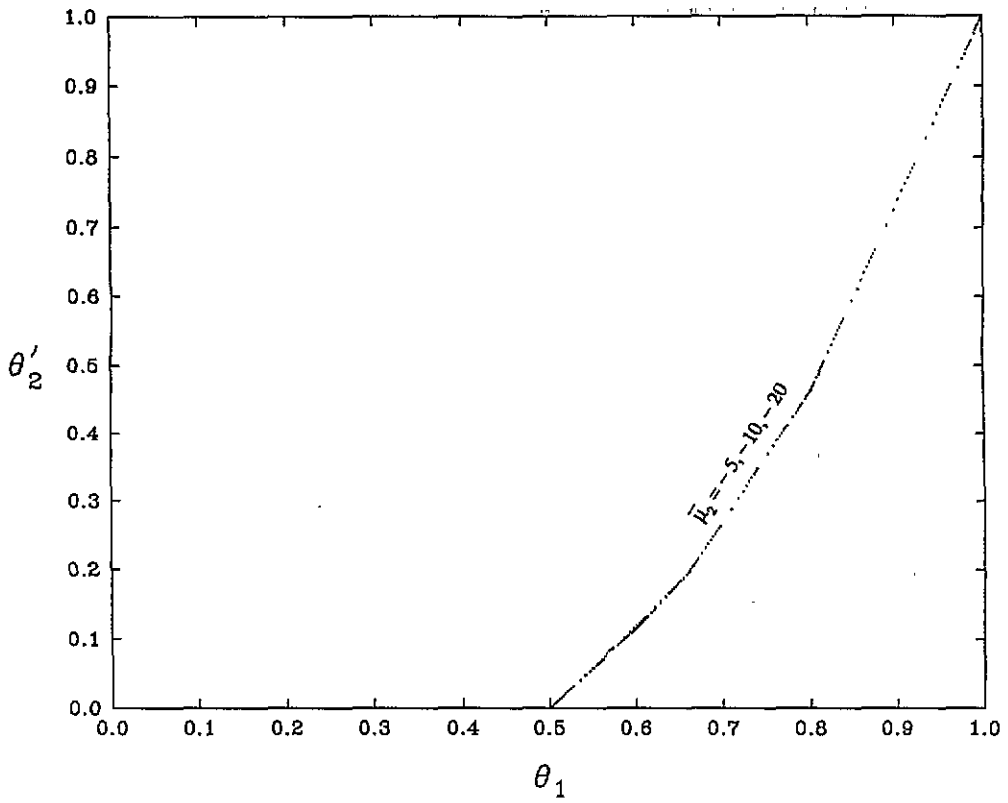


**Figure 16.** Plot of the fraction of the maximum number of nearest neighbours versus the coverage for the lattice of width $M = 5$.

entropy varies with the energy parameters, figure 20 gives the plot of $S$ versus $\bar{\mu}_2$ and $\bar{\mu}_2$, for $M = 4$, and is the analog of figure 4. Here, the data points at constant $\bar{\mu}_2$ are planar, and, for decreasing negative values of $\bar{\mu}_2$, are on curves exhibiting three valleys of increasing width, corresponding to the cusps of the plot of $S$ versus $\theta_1$. Consider the constant $\bar{\mu}_2$ curves for sufficiently repulsive dimer–dimer interaction. In that range, the curves of $\theta_2'$ versus $\theta_1$ are made of successive segments having different slopes, and the end points of any of these segments correspond to two consecutive cusps in the entropy curves. A local maximum of the entropy occurs between the two cusps when the energies are related according to equation (1.9). Thus, along a given segment mentioned above, the energies are related according to

$$\bar{\mu}_1 = -\left(\frac{\partial\theta_2}{\partial\theta_1}\right)_{x_2} \bar{\mu}_2 + \gamma. \tag{6.5}$$

Before the local maximum in the entropy $\gamma$ is negative, at the maximum it is zero, and after the maximum it is positive. At a point on a constant $\bar{\mu}_2$ curve located at the left and nearby a cusp, the energies are related according to an equation having the same form as (6.7) and with $\gamma$ positive. At a point on the same curve but to the right of the cusp and with the same entropy, the energies are related in a similar way but with $\gamma$ negative. Thus, in the vicinity of a cusp where the entropy is a local minimum, a given small change in the

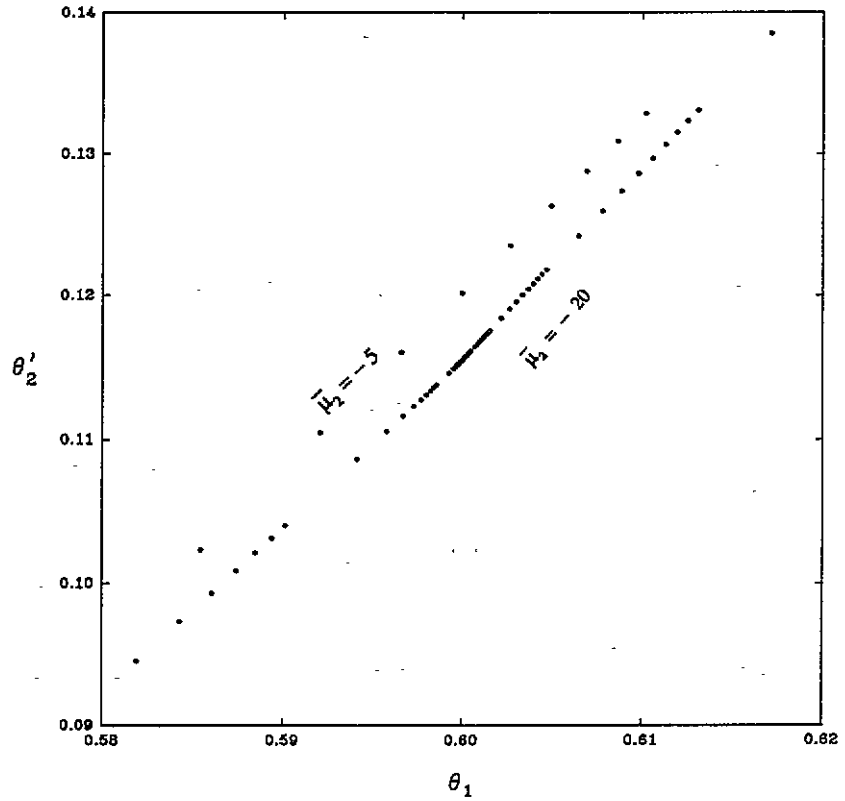


**Figure 17.** Enlargement of a portion of figure 16.

entropy changes $\Delta\bar{\mu}_1$ D in the lattice interaction energy by

$$\Delta\bar{\mu}_1 + \left[\left(\frac{\partial\theta_2}{\partial\theta_1}\right)_{x_2}^{\text{right}} - \left(\frac{\partial\theta_2}{\partial\theta_1}\right)_{x_2}^{\text{left}}\right]\bar{\mu}_2 + \left[\gamma_{\text{left}} - \gamma_{\text{right}}\right] = 0. \tag{6.6}$$

Respectively, *right* and *left* refer to the evaluation of the associated quantities just *after* and just *before* the cusp. The derivatives are readily obtained from table 2 and equation (6.4), and, since $\gamma_{\text{left}}$ is positive and $\gamma_{\text{right}}$ is negative, $[\gamma_{\text{left}} - \gamma_{\text{right}}] = \Delta\gamma$ is a positive quantity. Equation (6.6) has been verified numerically for every cusp and for all values of the lattice width $M$ under study. We obtained the values of $\Delta\gamma$ corresponding to changes in the entropy less than 0.5% of its minimum value at the cusp, when this minimum is not zero, and less than $1 \times 10^{-4}$ when this minimum is zero. For the cusp at 1/2 coverage, $\Delta\gamma = 27.5$, 29, 11.8 and 8.3 for $M = 2$, 3, 4 and 5, respectively; similarly, for the same values of $M$ at 2/3 coverage, $\Delta\gamma = 27$, 6.3, 11 and 3.7, respectively; for the cusp at 4/5 coverage, $\Delta\gamma = 28.9$ and 10.3 for $M = 4$ and 5; finally for the cusps at 3/5 ($M = 5$) and 6/7 ($M = 3$) coverages we have $\Delta\gamma = 9.3$ and 35.3, respectively.

## 7. Cusp configurations and the two-dimensional problem

Structural ordering at the cusps requires a repetitive pattern meeting the conditions given by the values of $\theta_1$ and $\theta_2'$ listed in table 3. Assume that this pattern occurs on a finite

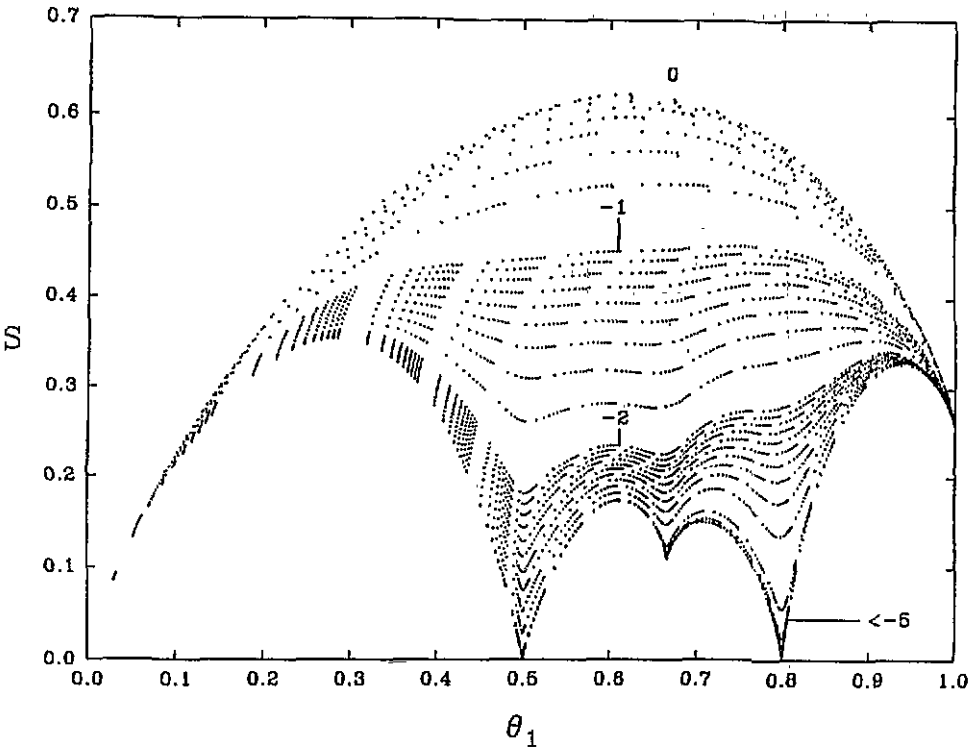


**Figure 18.** Plot of the entropy versus the coverage for the lattice of width $M = 4$.

section, $M \times N$, of the lattice. For that section, there are internal and external nearest neighbours. To avoid double counting, external nearest neighbours are those made across one of its boundaries. Let $B$ be the maximum number of nearest neighbours at full coverage of this section. Then, given $\theta_1$ and $\theta_2'$, the number $q$ of dimers and the number $b$ of nearest neighbours for that section are

$$B = 3(MN/2) - N \qquad q = \theta_1(MN/2) \qquad b = \theta_2' B. \tag{7.1}$$

In the subsequent analyses, we construct the lattice configurations prevailing at the cusps for $M \leqslant 5$, observe that cusp configurations for higher values of $M$ are made of configurations of lower values of $M$, extrapolate these configurations to lattices with $M > 5$, and obtain the existence of several cusps on the infinite two-dimensional lattice.

*Cusp at* $\theta_1 = 1/2$

The condition to be met is $\theta_2' = 0$ for $M = 2$, 3, 4 and 5, and, from equation (7.1), $b = 0$ and $q = MN/4$. A convenient choice for $N$ is 2 for $M$ even, and 4 for $M$ odd. All possible configurations are shown in figure 21 for $M = 2$, 3, 4 and 5.

For $M = 2$, there are four possible configurations of $2 \times 2$ sections each having two dimers and no nearest neighbours; these are called H, H′, V, and V′, with the primed configurations being the mirror image of the unprimed configurations. To complete the infinite $M = 2$ lattice, we consider a chain of these sections placed on top of one another. The sequencing selection rules are:

$$\mathrm{H} \to \mathrm{H}, \mathrm{H}', \mathrm{V}, \mathrm{V}';\ \mathrm{H}' \to \mathrm{H}';\ \mathrm{V} \to \mathrm{V}', \mathrm{H}';\ \mathrm{V}' \to \mathrm{V}, \mathrm{H}'.$$

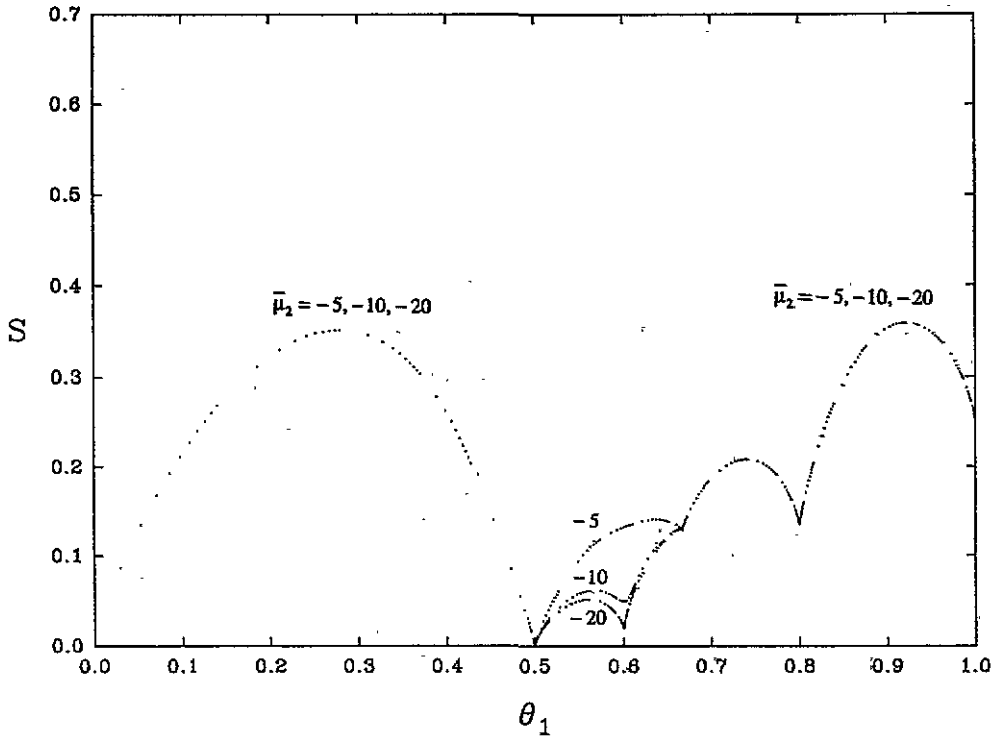


**Figure 19.** Plot of the entropy versus the coverage for the lattice of width $M = 5$.

From these rules, we may construct all the cusp configurations. In all subsequent discussions, we will generate the sequencing rules leading to the cusps configurations. Entropy is related to probability $(-P \ln P)$, therefore, when the number of cusp configurations is finite, this requires the entropy at the cusp to be zero, since there is an infinite number of total configurations. But an infinite number of cusp configurations, which is the case here, does not necessarily mean that the entropy is non-zero. Consider the lattice $2 \times N$, with the number of cusp configurations finite as is the total number of configurations. As $N \to \infty$, both numbers become infinite, their ratio approaches zero, and the entropy is zero, as verified numerically.

For $M = 3$, there are 12 possible configurations of $3 \times 4$ sections each having three dimers and no nearest neighbours. With label $j$ running from 1 to 5, these configurations are called $\mathrm{H}_j$, $\mathrm{H}'_j$, V, and V′, with the primed configurations being the mirror image of the unprimed configurations. The sequencing selection rules are:

$$\mathrm{H}_1 \to \mathrm{H}'_1;\ \mathrm{H}'_1 \to \mathrm{H}_1;\ \mathrm{H}_2 \to \mathrm{H}_1, \mathrm{H}'_2, \mathrm{H}_3, \mathrm{H}_4, \mathrm{V}'$$
$$H'_2 \to H'_1, H_2, V', H'_3, H'_4;\ H_3 \to H'_1;\ H'_3 \to H_1$$
$$H_4 \to V';\ H'_4 \to V';\ H_5 \to H'_1;\ H'_5 \to H_1$$
$$V \to V, H_1, H'_1, H_5, H'_5;\ V' \to V'.$$

For $M = 4$, there are four possible configurations, H, H′, V and V′, of $4 \times 2$ sections containing two dimers and no nearest neighbours. The sequencing selection rules are:

$$\mathrm{H} \to \mathrm{H}, \mathrm{H}' \to \mathrm{H}', \mathrm{V} \to \mathrm{V}', \mathrm{V}' \to \mathrm{V}$$

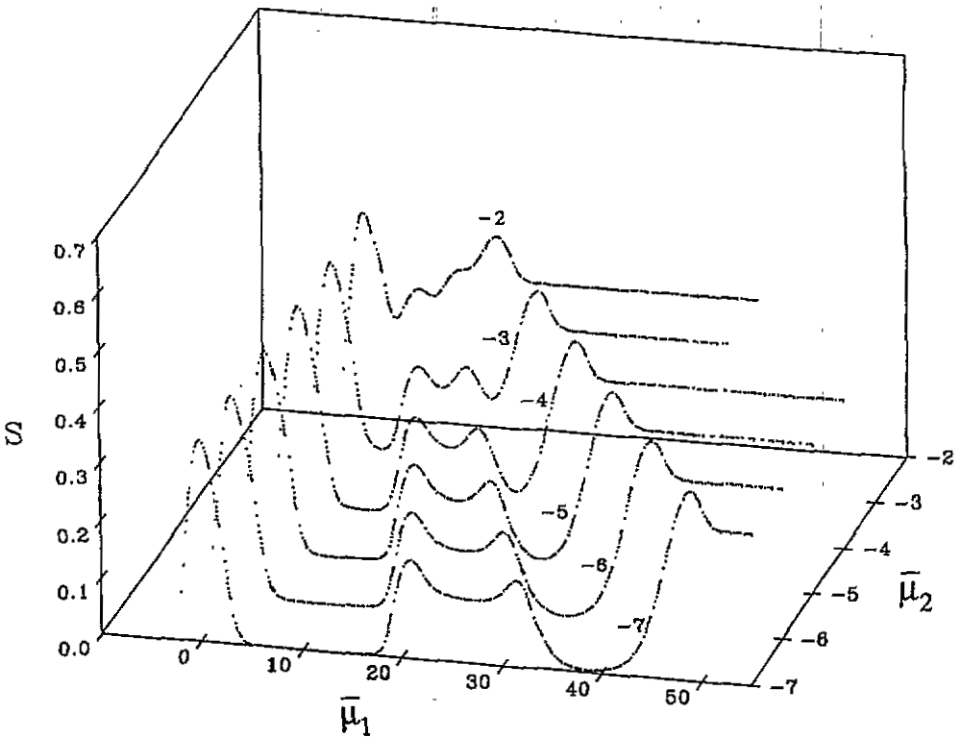


**Figure 20.** Plot of the entropy versus the dimensionless interaction energy parameters for the lattice of width $M = 4$.

**Table 3.** Location of the cusps observed in the entropy curves for lattices of widths $M = 1$, 2, 3, 4 and 5 as obtained numerically. Some of the graphical representations of these cusps are shown in figures 3, 18 and 19, for $M = 1$, 4 and 5, respectively.

| | $\theta_1 = 1/2$ | | $\theta_1 = 3/5$ | | $\theta_1 = 2/3$ | | $\theta_1 = 4/5$ | | $\theta_1 = 6/7$ | |
|---|---|---|---|---|---|---|---|---|---|---|
| | $S$ | $\theta_2'$ | $S$ | $\theta_2'$ | $S$ | $\theta_2'$ | $S$ | $\theta_2'$ | $S$ | $\theta_2'$ |
| M = 1 | | | | | 0 | 0 | | | | |
| M = 2 | 0 | 0 | | | 0 | 1/6 | | | | |
| M = 3 | 0 | 0 | | | 0.1461 | 4/21 | | | 0.0330 | 4/7 |
| M = 4 | 0 | 0 | | | 0.1097 | 1/5 | 0 | 11/25 | | |
| M = 5 | 0 | 0 | 0.0191 | 3/26 | 0.1283 | 8/39 | 0.1346 | 6/13 | | |

and we are locked into two possible configurations. Finally, for $M = 5$ there are two possible configurations, V and V′, with the sequencing selection rules

$$\mathrm{V} \rightarrow \mathrm{V}, \quad \mathrm{V}' \rightarrow \mathrm{V}'.$$

Cusp configurations for $M = 4$ and 5 are obtained by juxtaposing cusp configurations found for $M = 2$ and 3. Recursively, lattices with even and odd widths can be shown to have configurations composed of those for $M = 2$ and those for $M = 2$ and 3, respectively. A cusp will always occur at 1/2 coverage with zero entropy.

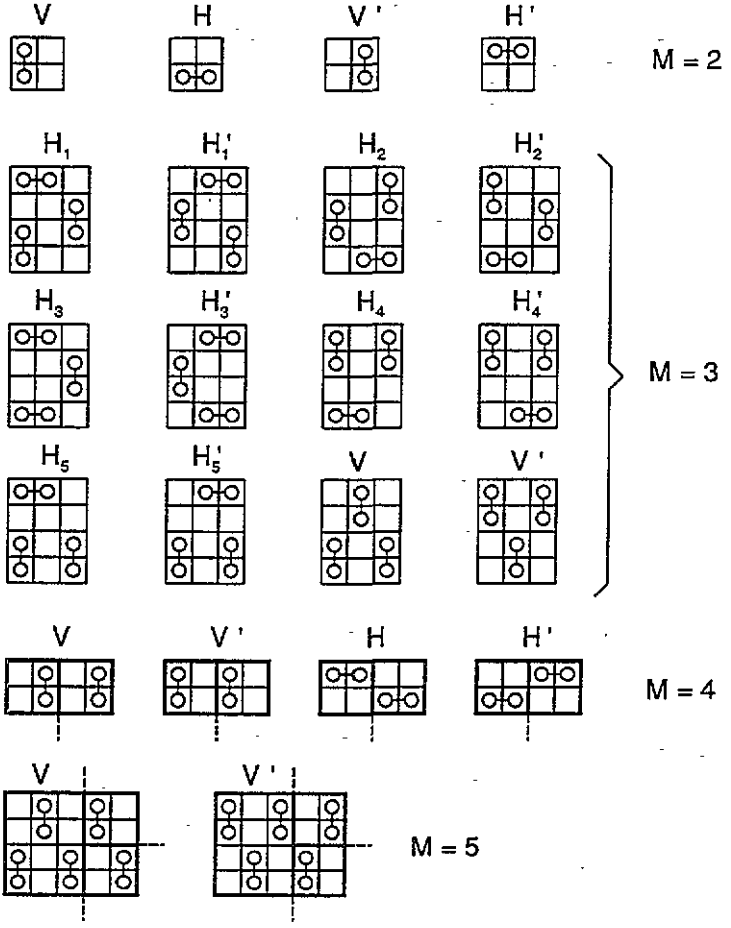


**Figure 21.** Cusp configurations of subsections of the lattices of widths $M = 2$, 3, 4 and 5 at 1/2 coverage.

*Cusp at* $\theta_1 = 2/3$

The condition to be met is $\theta_2' = 0$, 1/6, 4/21, 1/5, and 8/39 for $M = 1$, 2, 3, 4, and 5, respectively, and the relevant configurations are shown in figure 22.

The case $M = 1$ has been discussed earlier. For $M = 2$, equation (7.1) yields $2 \times N$ sections having $2N/3$ dimers and $N/3$ nearest neighbours, and we choose $N = 3$. There are two types of $2 \times 3$ sections, V and V', each having two dimers and one nearest neighbour. Note that these configurations are the juxtaposition of those found for $M = 1$. The sequencing selection rules are,

$$\mathrm{V} \rightarrow \mathrm{V}, \quad \mathrm{V}' \rightarrow \mathrm{V}'$$

there are two possible configurations, and the entropy is zero, as verified numerically.

For $M = 3$, equation (7.1) yields $3 \times N$ sections having $N$ dimers and $2N/3$ nearest neighbours, and we choose $N = 3$ leading to three dimers and two nearest neighbours per section. Two possibilities have to be considered. A section may have two internal and no external nearest neighbours; or, it may have one internal and one external nearest neighbour. There are four H-types and two V-types $3 \times 3$ sections with one and two internal nearest

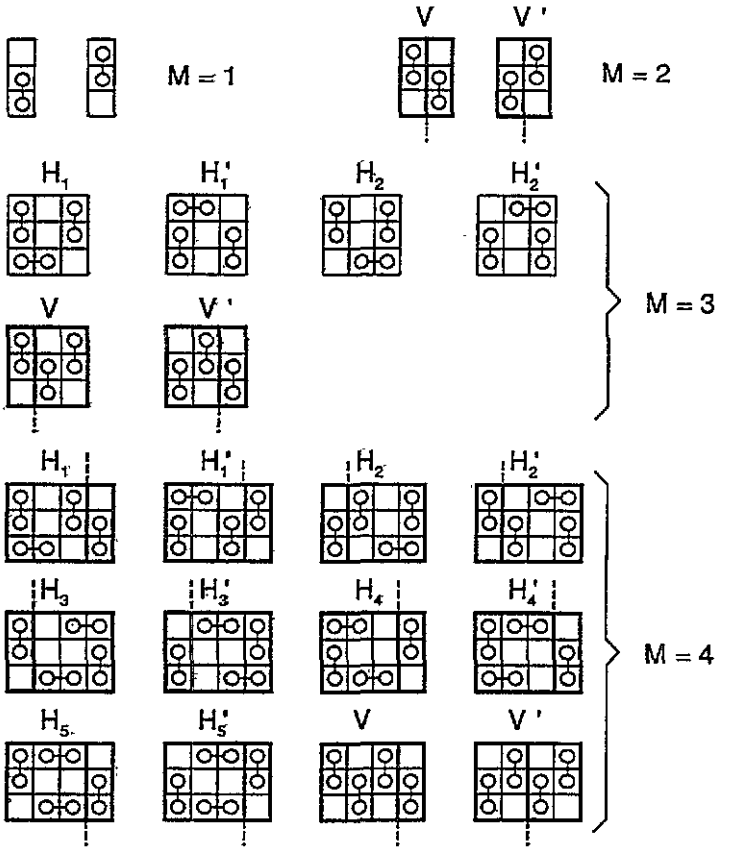


**Figure 22.** Cusp configurations of subsections of the lattices of widths $M = 1, 2, 3$, and 4 at 2/3 coverage.

neighbours, respectively. Here, only the V-type configurations are juxtaposed $M = 1$ configurations. The sequencing selection rules are

$$\mathrm{H}_1, \mathrm{H}_2 \to \mathrm{H}_1, \mathrm{H}_2, \mathrm{V};\ \mathrm{H}_1', \mathrm{H}_2' \to \mathrm{H}_1', \mathrm{H}_2'$$
$$V \to V;\ V' \to V', H_1', H_2'.$$

There is an infinite number of possible configurations at this cusp but this is not sufficient to prove that the entropy is not zero.

For $M = 4$, equation (7.1) yields $4 \times N$ sections having $4N/3$ dimers and N nearest neighbours, and we choose $N = 3$, leading to four dimers and three nearest neighbours. Here again there are two possibilities: three internal and no external nearest neighbours; or two internal and one external nearest neighbour. There are five H-types of $4 \times 3$ sections with two internal nearest neighbours and their mirror images, and one V-type section with three internal nearest neighbours and its mirror image. All the configurations are made of the juxtaposition of those found for $M = 1$ and 3; only the V-type can be viewed as made of those for $M = 1$. The sequencing selection rules are

$$H_1 \to H_1, H_3, H_4', H_5;\ H_2 \to H_2, H_3', H_4, H_5'$$
$$H_3, H_2', H_4', H_5' \to H_2', V;\ H_4, H_1', H_3', H_5 \to H_1', V'$$
$$V \to V, H_2';\ V' \to V', H_1'.$$

The same comments made for $M = 3$ at this cusp continue to be valid.

A similar analysis can be done for $M = 5$ and generalized to any $M$. As for the cusp at 1/2 coverage, we find that cusp configurations for $M > 5$ can be obtained by juxtaposing those found for $M = 1$ and 3. In particular, there will always be V-type configurations which are made of those for $M = 1$. It suffices to look at the V-type configurations: as $M$ increases by one unit, so does the number $b$ of nearest neighbours, starting with $b = 0$ for $M = 1$. Thus, using equation (7.1), we predict for any value of $M$ a cusp at 2/3 coverage with

$$\theta_2' = \frac{2}{3}\frac{M-1}{3M-2}. \tag{7.2}$$

The entropy is zero only for $M = 1$ and 2 since there is a finite number of configurations, but not for $M = 3$, 4, and 5. As in other calculations [4,5], the values of $S$ at this cusp are expected to oscillate with $M$. Preliminary results for $M = 6$ indicate a fast damping of these oscillations, and an extrapolation to the infinite two-dimensional lattice predicts a cusp at 2/3 coverage with $\theta_2' = 2/9$ and an entropy of 0.102.

*Cusp at* $\theta_1 = 4/5$

At 4/5 coverage, a cusp is found at $M = 4$ and 5, with $\theta_2' = 11/25$ and 6/13, respectively. The relevant configurations are shown in figure 23.

Equation (7.1) with $M = 4$ and the corresponding values of $\theta_1$ and $\theta_2'$ yields $q = (8/5)N$ and $b = (11/5)N$. Choosing $N = 5$ leads to a total of eight dimers to be distributed on $4 \times 5$ sections with 11 nearest neighbours. This latter number turns out to be the lowest possible number that one may have on $4 \times 5$ sections covered with eight dimers, and there are two ways this can be achieved. The corresponding two sections are called H and H' and have nine internal and two external nearest neighbours, and the sequencing selection rules are:

$$H \to H;\ H' \to H'.$$

There are two possible configurations achieving the conditions at this cusp, and the entropy is zero as verified numerically.

The case $M = 5$ is discussed in a similar way and we show in figure 23 two H-type sections from which two possible configurations are identified: sections H and H' can be arbitrarily connected by a one-unit height section containing two dimers separated by a vacancy. This partially justifies a non-zero entropy at this cusp.

The configurations for $M = 5$ cannot be obtained from those for $M = 4$. Those for $M = 4$ can be viewed as a juxtaposition of two $2 \times 5$ subsections each containing four dimers (figure 23). Each subsection has four internal nearest neighbours, one nearest neighbour shared with the other subsection, and another nearest neighbour at its top or bottom boundary. We can apply the same logic governing the generation of the cusps at 1/2 and 2/3 coverage. A cusp at 4/5 coverage is expected to occur at higher values of $M$ with configurations made of those at $M = 4$ and 5.

For a given cusp coverage, the number of nearest neighbours is at its minimum. With 4/5 coverage, the number $q$ of dimers is determined and a configuration is obtained by arranging the dimers with the least number of nearest neighbours. For $M = 6$, it is only possible to use $M = 4$ configurations made of the $2 \times 5$ subsections identified above. To keep nearest neighbours at their minimum, there is one shared nearest neighbour at one interface and three at the other. This is generalized to any even width $M > 6$. The number

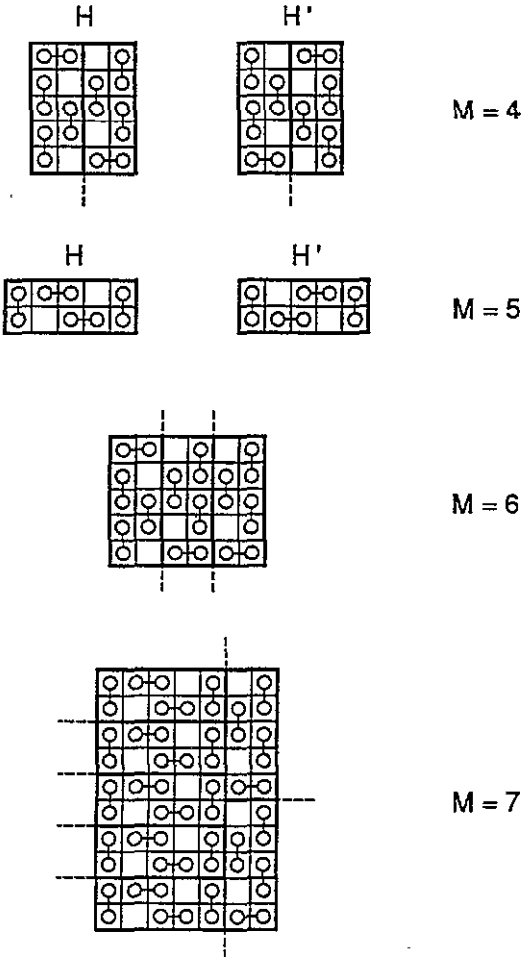


**Figure 23.** Cusp configurations of subsections of the lattices of widths $M = 4$, 5, 6 and 7 at 4/5 coverage.

of $2 \times 5$ subsections is $M/2$, each having one external and four internal nearest neighbours. They have $(M/2) - 1$ shared boundaries; at the first boundary there is one shared nearest neighbour, and at the remaining $(M/2) - 2$, there are three. This yields a total number $b$ of nearest neighbours:

$$b = 5(M/2) + 1 + 3[(M/2) - 2] = 4M - 5.$$

With $N = 5$ and $b$ given by this equation, equation (7.1) yields

$$\theta_1 = \frac{4}{5} \qquad \theta_2' = \frac{4M-5}{3M-2}. \tag{7.3}$$

Preliminary results for $M = 6$ show equation (7.3) to hold with no visible cusp. On the infinite lattice, we predict $\theta_2' = 8/15$ at 4/5 coverage, with no compelling reason to believe that it corresponds to a cusp.

Configurations for lattices with odd widths $M > 5$ can be obtained by juxtaposing sections with configurations found for $M = 4$ and 5. Figure 23 shows a configuration for $M = 7$ composed of five sections found for $M = 5$ and two right half-sections for $M = 4$.

The pattern repeats in $7 \times 10$ sections. In general, the pattern repeats in $M \times 5$ sections for $M$ even and $M \times 10$ sections for $M$ odd, and the value of $\theta_2'$ in both cases is given by equation (7.3).

*Cusps at $\theta_1 = 3/5$ and 6/7*

For $M = 3$, a cusp is found at 6/7 coverage and $\theta_2' = 4/7$, and for $M = 5$, a cusp is found at 3/5 coverage with $\theta_2' = 3/26$. Some configurations associated with these cusps are shown in figure 24. For $M = 3$, there are two configurations with sequencing selection rules $H_1, H_2 \rightarrow H_1, H_2$, leading to an infinite number of cusp configurations. For $M = 5$, the non-zero entropy requires the existence of several configurations, but we were able to find only one. The cusp at 6/7 coverage does not show up for $M = 4$ and 5, therefore we cannot make any predictions. As for the cusp at 3/5 coverage, no prediction is possible until numerical results are available for $M = 6$.

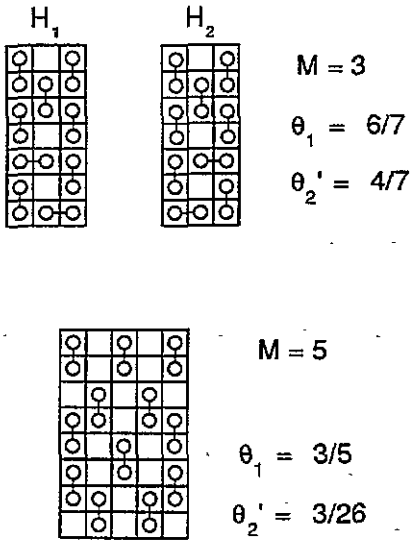


**Figure 24.** Cusp configurations of subsections of the lattices of widths $M = 3$ and 5 at 6/7 and 3/5 coverages, respectively.

## 8. Summary

The construction of the transfer matrix for the problem of dimers with nearest-neighbour interactions on an $M \times N$ square lattice is an essential step in the study of the thermodynamic properties of such a system. This matrix was constructed recursively from the knowledge of the matrices for $M = 1$ and $M = 2$ (figures 1, 5–12). Its largest eigenvalue raised to the power $1/M$ is the partition function of the system in the thermodynamic limit. The transfer matrix for the lattice of width $M$ is divided into block matrices, which can be further divided in a similar way, showing a fractal-like structure. This means that larger lattices include information contained in their constituent smaller lattices.

Eigenvalues of the transfer matrix can be obtained analytically only for the one-dimensional problem. We used EISPACK on the Cray C90 to carry out the numerical calculations. Computational difficulties presently preclude calculations for $M$ greater than 5. We varied the interaction energies and obtained the corresponding values of the coverage $\theta_1$, the fraction $\theta_2'$ of the maximum number of nearest neighbours and the entropy $S$. The

plots $\theta_2'$ versus $\theta_1$ (figures 2, 13–16) show that data points fall within a polygon. Beyond a certain repulsive dimer–dimer interaction energy ($\tilde{\mu}_2 < 0$), the points lie on the lower boundary of the polygon (table 2), whose vertices correspond to cusps on the constant-$\tilde{\mu}_2$ curves in the plot of $S$ versus $\theta_1$ (figures 3, 18 and 19). We find 1, 2, 3, 3, and 4 cusps for $M = 1$, 2, 3, 4, and 5, respectively. The pertinent characteristics of the cusps have been obtained and described, including coverage and fraction of the maximum number of nearest neighbours (table 3), energies (figures 4 and 20) and lattice configurations (figures 21–24). In particular, the amount of lattice energy required to break the structural ordering at the cusp is found to be linearly related to the repulsive energy between dimers (equation (6.6)). The local maxima of the entropy between cusps have been obtained and analysed (tables 4 and 5).

**Table 4.** Characteristics of the local maxima in the entropy curves for lattices of width $M = 2$, 3 and 4, and for values of the dimer–dimer interaction energy parameter in the range $\tilde{\mu}_2 < -5$.

| | Max. | # 1 | # 2 | # 3 | # 4 |
|---|---|---|---|---|---|
| | | $\mu_1 = 0$ | $\mu_1 = -2\mu_2$ | $\mu_1 = -5\mu_2$ | |
| | $S$ | 0.3664 | 0.1406 | 0.3824 | |
| $M = 2$ | $\theta_1$ | 0.3059 | 0.5885 | 0.8618 | |
| | $\theta_2'$ | 0 | 0.0885 | 0.6545 | |
| | | $\mu_1 = 0$ | $\mu_1 = -8\mu_2$ | $3\mu_1 = -14\mu_2$ | $\mu_1 = -7\mu_2$ |
| | $S$ | 0.3548 | 0.1900 | 0.2099 | 0.2749 |
| $M = 3$ | $\theta_1$ | 0.2906 | 0.6116 | 0.7410 | 0.9549 |
| | $\theta_2'$ | 0 | 0.1276 | 0.3392 | 0.8647 |
| | | $\mu_1 = 0$ | $\mu_1 = -3\mu_2$ | $2\mu_1 = -9\mu_2$ | $\mu_1 = -7\mu_2$ |
| | $S$ | 0.3536 | 0.1734 | 0.1497 | 0.3269 |
| $M = 4$ | $\theta_1$ | 0.2848 | 0.6121 | 0.7081 | 0.9364 |
| | $\theta_2'$ | 0 | 0.1346 | 0.2746 | 0.8219 |

**Table 5.** Characteristics of the local maxima in the entropy curves for the lattice of width $M = 5$ and for values of the dimer–dimer interaction energy parameter in the ranges $-7 \leqslant \tilde{\mu}_2 \leqslant -3$ and $\mu_2 \leqslant -15$.

| $M = 5$ | | $0 \leqslant \theta_1 \leqslant \frac{1}{2}$ | $\frac{1}{2} \leqslant \theta_1 \leqslant \frac{3}{5}$ | $\frac{3}{5} \leqslant \theta_1 \leqslant \frac{2}{3}$ | $\frac{2}{3} \leqslant \theta_1 \leqslant \frac{4}{5}$ | $\frac{4}{5} \leqslant \theta_1 \leqslant 1$ |
|---|---|---|---|---|---|---|
| | | $\mu_1 = 0$ | | $5\mu_1 = -16\mu_1$ | $\mu_1 = -5\mu_1$ | $\mu_1 = -7\mu_1$ |
| | $S$ | 0.3511 | | 0.1408 | 0.2084 | 0.3584 |
| $-7 \leqslant \tilde{\mu}_2 \leqslant -3$ | $\theta_1$ | 0.2791 | | 0.6370 | 0.7404 | 0.9220 |
| | $\theta_2'$ | 0 | | 0.1669 | 0.3469 | 0.7900 |
| | | $\mu_1 = 0$ | $\mu_1 = -3\mu_1$ | $2\mu_1 = -7\mu_1$ | $\mu_1 = -5\mu_1$ | $\mu_1 = -7\mu_1$ |
| | $S$ | 0.3511 | 0.0508 | 0.1293 | 0.2082 | 0.3584 |
| $\tilde{\mu}_2 \leqslant -15$ | $\theta_1$ | 0.2791 | 0.5603 | 0.6642 | 0.7404 | 0.9220 |
| | $\theta_2'$ | 0 | 0.0696 | 0.2019 | 0.3467 | 0.7900 |

The cusp at 2/3 coverage occurs for all values of $M$, and the cusp at 1/2 coverage occurs for $M > 1$. Cusp configurations on a lattice of width $M$ are composed of those found in lattices of smaller width (figures 21–22), keeping the number of nearest neighbours

at its minimum. This may be due to the fractal-like structure of the transfer matrix. Using this principle as a guide for any $M$, we predict the existence of at least two cusps at 1/2 coverage and $\theta_2' = 0$, and at 2/3 coverage and $\theta_2'$ given by equation (7.2). At 4/5 coverage we predict the value of $\theta_2'$ to be given by equation (7.3) for $M > 3$. Taking the limit $M \to \infty$, our speculation predicts for the infinite two-dimensional lattice the existence of at least two cusps; one at 1/2 coverage, no nearest neighbours, and zero entropy; and the other at 2/3 coverage, $\theta_2' = 2/9$, and an entropy of 0.102. In addition, we also predict that, at 4/5 coverage, $\theta_2' = 8/15$.

Further studies must be carried out for $M > 5$ to determine whether the cusps observed repeat and whether new cusps develop at higher values of $M$.

## Acknowledgments

One of us (AJP) would like to acknowledge the support received from NSF and the Pittsburgh Supercomputing Center, grant #PHY910014P.

## References

[1] Fowler R H and Rushbrooke G S 1937 *Trans. Faraday Soc.* **33** 1272
[2] Baxter R J 1982 *Exactly Solved Models in Statistical Mechanics* (New York: Academic Press)
[3] Lichtman D and McQuistan R B 1967 *J. Math. Phys.* **8** 2441
Mc Quistan R B 1968 *Il Nuovo Cim.* B **58** 86
McQuistan R B and LIchtman S B 1970 *J. Math. Phys.* **11** 3095
McQuistan R B and Hock J L 1983 *Fibonacci Quart.* **21** 196
Hock J L and McQuistan R B 1983 *J. Math. Phys.* **24** 1859
[4] Phares A J 1984 *J. Math. Phys.* **25** 1756; 25, 2169
Phares A J, Shaw D E and Wunderlich F J 1985 *J. Math. Phys.* **26** 1762
Phares A J and Wunderlich F J 1985 *J. Math. Phys.* **26** 2491
[5] Kasteleyn P W 1961 *Physica* **27** 1209; 1963 *J. Math. Phys.* **4** 287
Temperley H N V and Fisher M E 1961 *Philos. Mag.* **6** 1061
Fisher M E 1961 *Phys. Rev.* **124** 1664
Stephenson J 1964 *J. Math. Phys.* **5** 1009
Nagle J F 1966 *Phys. Rev.* **152** 190
Lieb E H 1967 *J. Math. Phys.* **8** 2339
Gaunt D S 1969 *Phys. Rev.* **179** 174
Heilmann O H and Lieb E H 1972 *Commun. Math. Phys.* **25** 190
Phares A J and Wunderlich F J 1986 *J. Math. Phys.* **27** 1099; *Il Nuovo Cim.* B **101** 653
Heise M 1989 *Physica* A **157** 953
Hosoya H and Balasubramanian K 1989 *Theor. Chim. Acta* **76** 315
Klein D J and Schmalz T G 1990 *Phys. Rev.* B **41** 2244
[6] Wojciechowski K W, Frenkel D and Branka A C 1991 *Phys. Rev. Lett.* **66** 3168
[7] Phares A J and Wunderlich F J 1987 *Phys. Lett.* A **127** 275; 1988 *Phys. Lett.* A **130** 385; *Phys. Lett.* A **133** 63
[8] Walikainen D and McQuistan R B 1985 *J. Math. Phys.* **26** 815
McQuistan R B and Hock J L 1986 *J. Math. Phys.* **27** 599
[9] Phares A J, Wunderlich F J, Grumbine D W and Curley J D 1993 *Phys. Lett.* A **173** 365